The Albedo of Fractal Stratocumulus Clouds

ROBERT F. CAHALAN, WILLIAM RIDGWAY,* WARREN J. WISCOMBE, AND THOMAS L. BELL

NASA/Goddard Space Flight Center, Laboratory for Atmospheres, Greenbelt, Maryland

JACK B. SNIDER

NOAA/ERL/Wave Propagation Laboratory, Boulder, Colorado

(Manuscript received 23 June 1993, in final form 25 February 1994)

ABSTRACT

An increase in the planetary albedo of the earth–atmosphere system by only 10% can decrease the equilibrium surface temperature to that of the last ice age. Nevertheless, albedo biases of 10% or greater would be introduced into large regions of current climate models if clouds were given their observed liquid water amounts, because of the treatment of clouds as plane parallel. Past work has addressed the effect of cloud shape on albedo; here the focus is on the within-cloud variability of the vertically integrated liquid water. The main result is an estimate of the "plane-parallel albedo bias" using the "independent pixel approximation," which ignores net horizontal photon transport, from a simple fractal model of marine stratocumulus clouds that ignores the cloud shape. The use of the independent pixel approximation in this context will be justified in a separate Monte Carlo study.

The focus on marine stratocumulus clouds is due to their important role in cloud radiative forcing and also that, of the wide variety of earth's cloud types, they are most nearly plane parallel, so that they have the least albedo bias. The fractal model employed here reproduces both the probability distribution and the wavenumber spectrum of the stratocumulus liquid water path, as observed during the First ISCCP Regional Experiment (FIRE). The model distributes the liquid water by a cascade process, related to the upscale cascade of energy transferred from the cloud thickness scale to the mesoscale by approximately 2D motions. For simplicity, the cloud microphysical parameters are assumed homogeneous, as is the geometrical cloud thickness; and the mesoscale-averaged vertical optical thickness is kept fixed at each step of the cascade. A single new fractal parameter, $0 \leq f \leq 1$, is introduced and determined empirically by the variance of the logarithm of the vertically integrated liquid water. In the case of conservative scattering, the authors are able to estimate the albedo bias analytically as a function of the fractal parameter f, mean vertical optical thickness τ_v, and sun angle θ. Typical observed values are $f = 0.5$, $\tau_v = 15$, and $\theta = 60°$, which give an absolute bias of 0.09, or a relative bias equal to 15% of the plane-parallel albedo of 0.60. The reduced reflectivity of fractal stratocumulus clouds is approximately given by the plane-parallel reflectivity evaluated at a reduced "effective optical thickness," which when $f = 0.5$ is $\tau_{eff} \approx 10$.

Study of the diurnal cycle of stratocumulus liquid water during FIRE leads to a key unexpected result: the plane-parallel albedo bias is largest when the cloud fraction reaches 100%, that is, when any bias associated with the cloud fraction vanishes. This is primarily due to the variability increase with cloud fraction. Thus, the within-cloud fractal structure of stratocumulus has a more significant impact on estimates of its mesoscale-average albedo than does the cloud fraction.

1. Introduction

Many theoretical studies have shown the sensitivity of cloud radiative properties to their spatial structure, ranging from the seminal work of McKee and Cox (1974) and Stephens (1976) to more recent work by Harshvardan and Weinman (1982), Welch and Wielicki (1985), and others. As Harshvardan and Randall (1985) have pointed out, current general circulation models, because of their reliance on plane-parallel assumptions, are in the embarrassing situation of having to use unrealistically small liquid water amounts to produce realistic albedos. Stephens (1985) has emphasized that the mean albedo is not a function of mean liquid water alone, but also depends upon its spatial distribution, and has provided a general formalism to account for spatial inhomogeneity (Stephens 1988a,b). Lovejoy (1982) suggested that cloud spatial distributions may be modeled by self-similar fractals and, with Schertzer and other collaborators, has more recently generalized to multifractals [see, for example, Lovejoy et al. (1990) and Schertzer and Lovejoy (1987), and

*Additional affiliation: Applied Research Corporation, Landover, Maryland.

Corresponding author address: Dr. Robert F. Cahalan, Code 913, Laboratory for Atmospheres, Goddard Space Flight Center, Greenbelt, MD 20771.

references therein]. Cahalan (1989) employed a simple multifractal model to show that the area-averaged albedo is insensitive to scales smaller than a photon mean free path, typically on the order of 100 m. Rhys and Waldvogel (1986) and others have shown that cloud fractal dimensions undergo abrupt changes at certain scales, and Cahalan and Joseph (1989) found that these characteristic scales depend on cloud type and brightness threshold.

Two cloud types that have been the focus of particular attention recently are cirrus and marine stratocumulus. Conventional wisdom is that cirrus, being high and optically thin, act mainly to decrease the outgoing longwave radiation and thus have a net heating effect, while marine stratocumulus, being low and optically thicker, primarily cool the climate. However, to quantify these two effects will require careful estimates of the thermal emissivity and reflectivity of both cirrus and marine stratocumulus clouds. A central result of the Earth Radiation Budget Experiment is that *net* cloud radiative forcing is maximum at the locations and seasons of extensive marine stratocumulus, and is dominated by the shortwave reflection (Harrison et al. 1990; Ramanathan et al. 1989; see also Hartmann and Short 1980). Reflection estimates are affected both by the microstructure of cloud fields (drop sizes, absorption, etc.) and by their macrostructure (cloud fraction, cloud variability, etc.). Here we focus upon the macrostructure of marine stratocumulus, and its impact on reflectivity.

Marine stratocumulus are perhaps the closest of any cloud type to plane parallel. They are typically 200–400 m thick, being confined in the vertical between the lifting condensation level and the strong subtropical inversion, while covering horizontal areas 1000 km or more in diameter. Their cloud fractions often approach 100% over large regions of subtropical eastern ocean basins, particularly in summer. The question naturally arises: How accurate are plane-parallel estimates of stratocumulus reflectivity, which form the basis of approximations used in current general circulation models (GCMs), and are also fundamental to algorithms used in satellite retrievals of cloud properties? These are really two distinct questions, since GCMs and satellite retrievals operate at very different spatial resolutions. Retrievals typically assume that the brightness of each 1-km pixel is a function only of the properties within that pixel's field of view. We shall make a similar assumption in this paper, and justify it for 100% marine stratocumulus in a separate Monte Carlo study. GCMs, on the other hand, try to determine at each time step the mean properties over a field of view 100 km or more in diameter and artificially compensate for the effect of subgrid-scale variations. The main purpose of this paper is to estimate the error GCMs make in treating clouds as uniform over the mesoscale.

The plane-parallel albedo biases estimated in this paper are based on a fractal model that reproduces the wavenumber spectrum and probability distribution of integrated liquid water inferred from observations of stratocumulus clouds observed in the First International Satellite Cloud Climatology Regional Field Experiment (FIRE) in 1987. Several results do not depend on the specific fractal model or the particular observations, but are more generally true. First, the area-average albedo of an inhomogeneous cloud field is less than that of a uniform cloud having the same microphysical parameters and the same total liquid water. Thus, the plane-parallel albedo bias is always positive for conservative scattering in the IPA. Second, the albedo bias is more sensitive to the *within-cloud variance* of the cloud liquid water than it is to the mean. Third, the within-cloud variance becomes increasingly important as the cloud fraction increases. For stratocumulus, the impact of within-cloud variance is enhanced by the fact that the variance increases with cloud fraction, and in fact the bias is maximum when the cloud fraction reaches 100%.

The outline of the paper is as follows. The following section provides some background—it first discusses the sensitivity of the global energy balance to changes in the global albedo and then describes the relevant observations of marine stratocumulus clouds. Section 3 introduces a simple "bounded cascade" model of stratocumulus cloud optical depth and some related assumptions, and gives a first rough estimate of the albedo bias. This bias is found to be significant when model parameters are estimated from observations. Section 4 describes the dependence of the bias on mean optical depth, sun angle, and fractal variability for the case of conservative scattering in overcast stratocumulus, and section 5 generalizes these results to include absorption. Section 6 examines the diurnal cycle of cloud fraction and within-cloud variability and shows that the within-cloud variability has more impact on the diurnal cycle of the albedo bias than does cloud fraction. Section 7 summarizes the results and discusses possible extensions. Finally, appendix A provides a simple derivation of the $k^{-5/3}$ wavenumber spectrum of the bounded cascade model; appendix B outlines derivations of the model's statistical moments; appendix C gives simple upper and lower bounds for cloud optical thicknesses in the bounded cascade model; and appendix D describes a simple analytic reflection function for conservative scattering.

2. Preliminaries

a. Global sensitivity to cloud albedo changes

Before attempting to estimate the bias associated with plane-parallel albedo estimates, let us first consider what impact a given albedo bias might have upon the large-scale climate. [For related discussions, see, e.g., Wetherald and Manabe (1980) and Cahalan and Wiscombe (1993).] To that end, consider the global energy balance of the earth:

$$(1 - \alpha)(\text{solar constant})/4 = \sigma T_{\text{eff}}^4, \quad (2.1)$$

where α is the global average albedo, σ is the Stefan–Boltzmann constant, and T_{eff} is the mean radiative temperature of the earth. Here T_{eff} is determined by an average over cloud-free regions, where the radiative temperature approaches that of the surface, and cloudy regions, where the radiative temperature can be as low as that of the tropopause.

One of the difficulties in determining the effect of clouds on climate is that an increase in cloud amount increases the albedo but also decreases T_{eff} and thus decreases both sides of the above energy balance, which can lead to either warming or cooling at the surface. In this paper we focus on stratocumulus clouds, which have been shown to be the major contributor to net cloud radiative forcing. They have low cloud tops and thus do not significantly decrease T_{eff}. Thus, they act mainly through their albedo.

Several empirical studies have shown that for monthly or annual averages, the right-hand side of (2.1) may be parameterized in terms of the equilibrium surface temperature as follows:

$$\sigma T_{\text{eff}}^4 = 208 + 2T_s, \quad (2.2)$$

where the surface temperature T_s is given in degrees Celsius, and the result is in watts per square meter (see, e.g., Short et al. 1984). Consider now a small change in the albedo, $\Delta\alpha$. From (2.1) and (2.2), with the current solar constant of 1360 W m^{-2} and global albedo of about 0.3, we find

$$\Delta T_s = -0.5°\text{C}\left(100\,\frac{\Delta\alpha}{\alpha}\right). \quad (2.3)$$

In other words, for each 1% decrease in the mean albedo (i.e., an absolute albedo bias of about 0.003), the equilibrium surface temperature warms by 0.5°C. A 10% albedo drop, from 0.30 to 0.27, would produce a global warming equivalent to the 5°C warming experienced since the last ice age.

Clearly, this means that 10% albedo errors are unacceptably large when they extend over climatic time and space scales. We shall see below that for a given amount of cloud liquid water, plane-parallel models of stratocumulus have an absolute albedo bias of ~0.1. The fractional global coverage of stratocumulus and other "low clouds" has been estimated at ~25% (Hartmann et al. 1992). If all such clouds have the 0.1 bias estimated here, the resulting absolute bias in global albedo is 0.025, which is 8% of the global albedo. Larger albedo biases are expected for other cloud types, but these have smaller fractional coverage, and may also have compensating emissivity biases. GCMs avoid the large errors in regional surface temperature or horizontal heat flux implied by such plane-parallel albedo biases by either adjusting the albedo directly, thus effectively decoupling the cloud liquid from the cloud radiation, or introducing a compensating negative bias in the cloud liquid water. In this paper we show that the compensating liquid water bias is computable from a "reduction factor" χ that depends on the cloud fractal properties, which undergo diurnal and presumably also seasonal and geographical variations.

b. *Observations of stratocumulus liquid water*

Although marine stratocumulus clouds are often thought to be the premier example of plane-parallel clouds because of their large horizontal extent (sometimes exceeding 1000 km) and small thickness (less than 1 km), measurements of their liquid water reveal a highly turbulent structure, particularly at cloud top where it most affects the albedo. A study of marine stratocumulus by Cahalan and Snider (1989), based on data from the FIRE field program (summarized by Albrecht et al. 1988), found that the power spectrum of vertically integrated liquid water (W), as a function of wavenumber k, follows a $k^{-5/3}$ power law from the mesoscale down to the cloud thickness scale of a few hundred meters. Landsat reflectivity data indicate that this may change to k^{-3} at smaller scales, but this has not yet been confirmed with higher-resolution W data. Such a change in scaling at a few hundred meters may be a dynamical effect related to the strong subtropical inversion, or a purely photon mean free path effect (Barker and Davies 1992). In any case, theoretical computations (Cahalan 1989) show that the photon field tends to smooth out variations on scales smaller than the photon mean free path of 100 meters or so. The scales that matter most to the large-scale albedo are those larger than a few hundred meters, and there the $k^{-5/3}$ behavior of the liquid water spectrum is well established. If liquid water were a passive scalar field in a two-dimensional turbulent flow, this mesoscale power-law behavior could be associated with the upscale cascade of energy from the cloud scale (see, e.g., Gage and Nastrom 1986). Some model studies show that W fluctuates with the vertical velocity (e.g., McVean and Nicholls 1988), but whether W can be treated as effectively "passive" on these scales deserves further study. For the purposes of this paper, however, we shall simply assume the observed power-law behavior, and focus upon its consequences for the mesoscale-averaged albedo.

The accuracy of the independent pixel approximation, introduced in the next section, depends on the rapid falloff of the power spectrum. Monte Carlo studies, reported separately, show that corrections to the IPA are small in the $k^{-5/3}$ case, but become important when the spectrum flattens to k^{-1}. Thus, corrections to the IPA depend on two-point correlations as measured by the spectrum, as well as higher-order correlations. However, the IPA albedo itself is independent of the spectrum. In the IPA, the only property of the vertically integrated liquid water that matters is the one-point

probability distribution. That is, the IPA depends only on the probability of finding a certain fluctuation in the liquid water, not on how the fluctuations are partitioned by wavenumber, or how they are arranged in space. Spatial information is needed in order to *justify* the IPA, but not in order to compute it.

The one-point probability distribution function (PDF) of W, computed from FIRE observations, is shown in Fig. 1. This is based on measurements taken at 10 Hz and averaged for 1 min by the NOAA upward-looking 3-channel microwave radiometer on San Nicolas Island during 1–19 July 1987. The accuracy of these measurements has been discussed by Snider (1988), and the instrument itself is described in Hogg et al. (1983). Although the instrument can detect down to about 2 g m^{-2}, the smaller values are more uncertain. We will isolate these uncertainties by assuming that values below 10 g m^{-2} are "cloud-free." The mean and variance of the values of $\log(W)$ above that threshold are shown in the figure, along with a lognormal fit and a fit based on the bounded cascade model described in section 3.

The FIRE observations on which Fig. 1 is based were affected by their proximity to land. Satellite measurements show that the mean optical thickness decreased from 12 to 10 from southeast to northwest through the island (Minnis et al. 1992). However, calculations show that the albedo *bias* due to the fractal structure is much less sensitive to the *mean* liquid water and optical thickness than to the *variability* of these quantities, as we shall see. We show below that the mean and variability were correlated diurnally on the island, suggesting that the variability may also be slightly less farther offshore, in which case the bias would also be slightly less.

In plane-parallel theory, only the mean of the W distribution is used to estimate the reflectivity. A central theme of this paper is that the mean fluxes are sensitive to the *variance* of the cloud optical thickness, and not only the mean. Subgrid-scale cloud variability is currently represented in GCMs by the "cloud fraction." For stratocumulus in particular, however, we shall see that the *within-cloud* variance matters more than the cloud fraction. The IPA takes account of the within-cloud variance, and in the bounded cascade model it is parameterized by the fractal parameter f, which determines the width of the distribution in Fig. 1, as indicated by the value of std dev$[\log(W)]$. This variance has a diurnal variation, as discussed in section 6, and presumably also annual and geographical variations that are not yet known. Clearly, much more climatological information is needed on this fundamental quantity, not only for the various stratocumulus regimes but also for other cloud types.

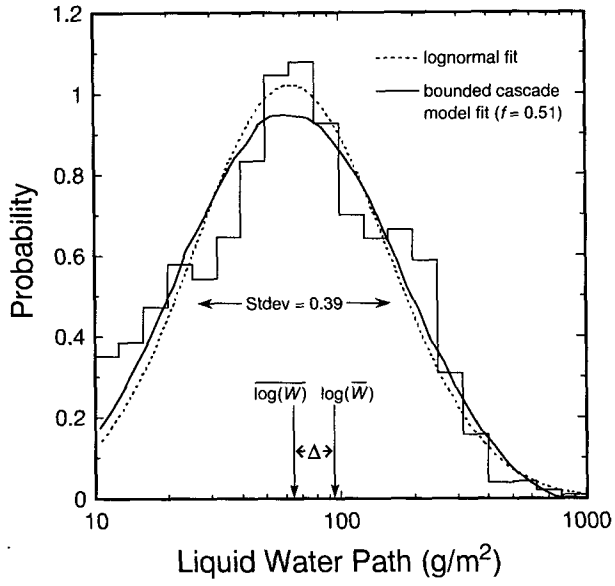

FIG. 1. Probability density of vertically integrated liquid water path W [g/m^2] is shown by the solid histogram, computed from 18 days of one-minute averaged data acquired during the July 1987 FIRE field program from the NOAA/WPL upward-looking 3-channel microwave radiometer on San Nicolas Island. Values below 10 g m^{-2} are assumed cloud-free, and the histogram is divided by the total number of counts above this threshold. The $N = 18\,907$ values are binned in 25 equally spaced bins between $\log W = 1$ and $\log W = 2.5$. The horizontal line shows the range of values within one standard deviation of $\overline{\log W}$, and the vertical lines show the spacing between $\overline{\log W}$ and $\log\bar{W}$, namely, Δ defined by (3.7). The dashed curve is a lognormal with the same mean and variance, and the solid curve is the bounded cascade model distribution with the same mean and variance, obtained from a realization having $f = 0.51$.

3. Assumptions and the bounded cascade model

In order to estimate the bias in plane-parallel estimates of stratocumulus cloud albedo, we shall make three main simplifying assumptions: the IPA, constant effective droplet radius, and the bounded cascade model. Let us consider these in order.

The first simplifying assumption is the "independent pixel approximation" or IPA (Cahalan 1989), in which the reflectivity of each cloud pixel depends only on the vertical optical thickness of that same part and not on the optical thickness of neighboring regions. In other words, we neglect any *net* horizontal photon transport. This approximation is not generally true, but can be shown to give the reflected flux of the bounded cascade model to better than 1%, as shown in a separate paper (Cahalan et al. 1994). The IPA is accurate when the spectrum falls off rapidly enough that the variability is sufficiently concentrated in the largest scales, as with the $k^{-5/3}$ spectrum of the bounded model.

Note that while purely plane-parallel computations depend only on the *mean* macro- and microphysical properties of the cloud, the IPA depends upon all the moments of the one-point distribution of cloud liquid water, as is seen below in Eq. (3.10), for example. Thus, it is not correct to refer to the IPA simply as a "plane-parallel" computation, although this confusion has sometimes appeared in the literature. Note also that

the IPA is not being applied here to a field of uniform clouds with some fixed size and shape, but rather to a cloud field having horizontal variations in the interior optical properties over a wide spectrum of scales, as further discussed below.

Our second simplifying assumption is that the effective droplet radius, r_{eff}, is constant, independent of W, and independent of the cloud fractal structure. Many studies have shown the dependence of r_{eff} on liquid water, location in the cloud, and other cloud parameters. Much less attention has been given to the cloud macrostructure. In order to devote full attention to the cloud macrostructure, we shall ignore all spatial variations in the microstructure. In particular, we shall set $r_{\text{eff}} = 10$ μm. Since the mean vertical cloud optical thickness τ_v is related to the cloud liquid water path W, as

$$\tau_v = \frac{3}{2}\frac{W}{r_{\text{eff}}},$$

where W is given in grams per square meter and r_{eff} is given in micrometers (Stephens 1976), we obtain the simple linear relation

$$\tau_v = 0.15W. \tag{3.1}$$

Typical values for stratocumulus are $W = 90$ g m^{-2} and $\tau_v = 13$, for a typical cloud thickness of 300 m (see, e.g., Fig. 1).

Fairall et al. (1990) applied a detailed radiative model to extended time observations during FIRE, and found an approximately linear relation like (3.1). Nakajima et al. (1991) obtained $r_{\text{eff}} \approx 10$–$15$ μm, from scanning radiometer measurements taken during ER-2 flights over the FIRE stratocumulus. They found a tendency for r_{eff} to increase with W on days with thin stratocumulus, and a slight tendency in the opposite direction on days with thick stratocumulus. The combined data from all days is consistent with the simple equation given above. [It is also necessary to combine a number of days of data in order to reveal the skewness in the W distribution, since some days have only thin or no clouds, and some days show a bimodal W distribution, perhaps associated with decoupled cloud and subcloud layers.]

While W is inferred from the microwave observations, τ_v is more appropriate for discussing radiative computations. Actually, we shall see that the most convenient radiative variable is the *logarithm* of the vertical optical thickness, because the reflection function then becomes approximately linear, so that the mean reflection is approximately the reflectivity of the mean logarithm, which leads to a simple "effective thickness approximation." Use of the logarithm also has the convenient feature that the rescaling in (3.1) will not affect the statistical moments. In all later equations, then, τ_v is equivalent to W through (3.1).

a. Bounded cascade model

Our third simplifying assumption is that a two-parameter multiplicative fractal cascade model describes the stratocumulus cloud liquid water distribution. One parameter, the "scaling parameter," $c = 2^{-1/3}$, is fixed by the $k^{-5/3}$ wavenumber spectrum observed during the FIRE stratocumulus field experiment (Cahalan and Snider 1989). The remaining free parameter, the "variance parameter" f, is determined by the variance of the logarithm of the cloud liquid water path, which depends on the season and time of day, as well as on the cloud type. Cahalan (1989) and Davis et al. (1991) have previously considered the radiative properties of multifractal cloud models, in which the cloud elements are concentrated on a fractal set of zero measure. Such a model can be obtained from the one considered here in the limit $c \to 1$. We refer to the model contained in that limit as the "singular model," while the one we focus on here is the "bounded model." Even though the bounded model does not have the same scale invariance as the singular model, its wavenumber spectrum is still a power law, as shown in appendix A. The general class of bounded cascades has self-affine scaling properties, nontrivial structure functions, and nonstationary multifractal properties (Marshak et al. 1994). The statistical moments of the bounded model are derived in appendix B, which also discusses the singular limit. A simple upper bound for the bounded model distribution is derived in appendix C. [Mandelbrot (1983) discusses a similar class of fractals in his chapter 15, and also in Mandelbrot (1986). For an earlier application of fractals to "clouds" generated by a passive scalar in two-dimensional turbulence, see Welander (1955).]

We will describe the model in its simplest form, which produces a fractal in only one horizontal direction, with rescalings by powers of 2. Generalizations to higher dimensions and other rescalings are straightforward. According to the IPA, more complex models that also fit the observed PDF (Fig. 1) will have the same mean albedo as computed here from the simple model. However, the PDF alone is not sufficient to determine the corrections to the IPA, which depend on two-point quantities such as the wavenumber spectrum. Such corrections turn out to be small for the parameter values considered here (Cahalan et al. 1994). The model proceeds as follows (see Fig. 2): begin with a plane-parallel cloud slab, with a fixed thickness in the vertical direction and in one horizontal direction, and infinite in the other horizontal direction (out of the paper in Fig. 2). Divide the slab in half lengthwise, and transfer a fraction of liquid water, f_0, from one half to the other, with the direction of transfer chosen randomly with equal probability. Next treat each of the two halves in the same way: divide each in half, and transfer a fraction of liquid water, f_1, from one quarter-slab to the neighboring one, with the transfer directions

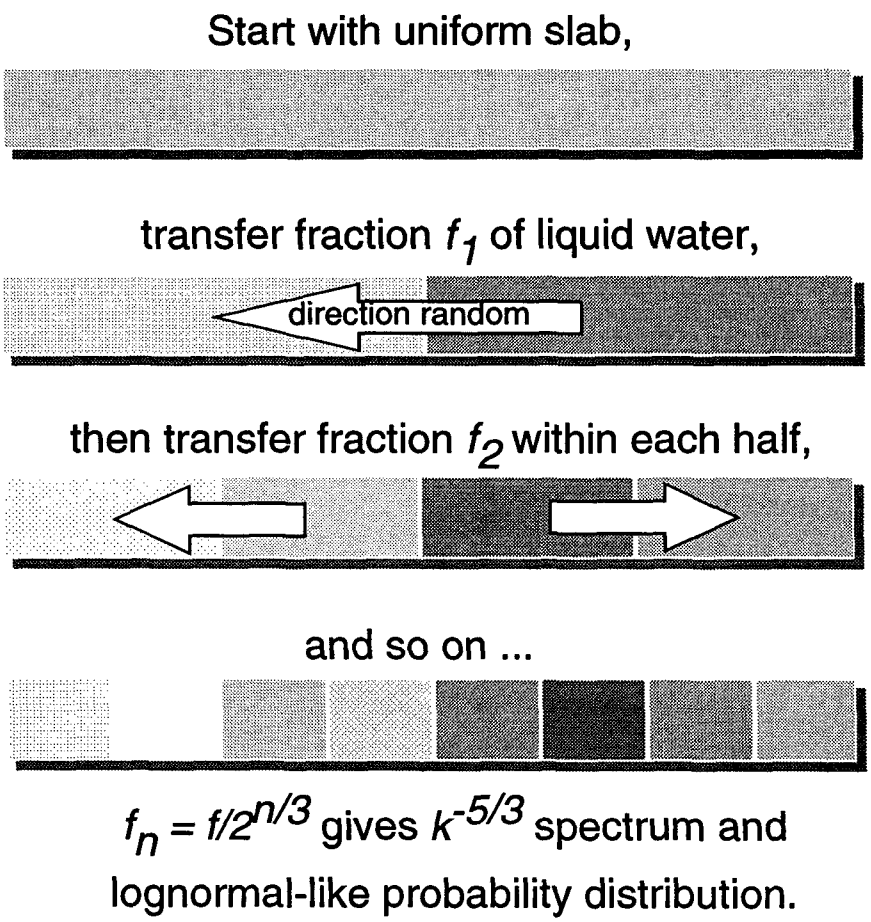

FIG. 2. Schematic description of the bounded cascade model. For simplicity, the cloud inhomogeneity is restricted to one horizontal direction. The generating process begins with (a) a uniform plane-parallel cloud that is infinite in one horizontal direction (out of the page) and has a large but finite optical thickness in the perpendicular horizontal direction and a moderate vertical optical thickness. This slab is then divided in half in the horizontally finite direction, and a fraction f_0 of liquid water is transferred from one half, chosen at random, to the other, producing two uniform slabs, as shown in (b). The total cloud liquid water and the average vertical optical depth are unchanged. Each of the two halves is then divided in the same way, and liquid water fractions f_1 are transferred within each half. The quarters are then halved, and so on down to the available resolution. The "singular model" has f_n independent of n and the power spectrum falls slower than k^{-1}, while the "bounded model" has $f_n = fc^n$ and the power spectrum falls faster than k^{-1} and has a $k^{-5/3}$ spectrum when $c = 2^{-1/3} \approx 0.8$.

chosen randomly and independently. Continue the procedure by halving each of the quarter-slabs, transferring f_2 among eighth-slabs, and so on. In appendix A, it is shown that if we let

$$f_n = fc^n, \tag{3.2}$$

then the resulting distribution of W (or τ_v) has a power-law wavenumber spectrum $S(k) \sim k^{-\alpha}$, where the exponent is given by $\alpha = 1 - \log_2(c^2)$, independent of the value of f so long as $c < 1$. Thus, a $k^{-5/3}$ spectrum is obtained by setting

$$c = 2^{-1/3} \approx 0.8. \tag{3.3}$$

From here on, it is assumed that (3.3) holds, so that the only remaining free fractal parameter is f, which will be determined empirically from the standard deviation of $\log(W)$.

For convenience, we have described the cascade beginning with the largest scales and proceeding to the smallest, because we want to begin by computing the plane-parallel albedo and see how this is affected by the smaller scales. It is important to remember, however, that the horizontal redistribution of liquid water is accomplished by turbulent mesoscale motions that are predominantly two-dimensional and are thought to be associated with an *upscale* cascade, in which energy cascading up from convective scales eventually merges with the energy cascading down from baroclinic scales. (See, e.g., Ca-

halan and Snider 1989; Gage and Nastrom 1986; Kraichnan 1967.) Lilly (1989) has shown that no mesoscale energy sink is needed to absorb the convective energy, which simply becomes submerged in the baroclinic activity at scales of several hundred kilometers.

Note that the total water, and thus the horizontal average liquid water path, $\bar{W}$, is kept fixed at each step of the cascade. However, the mean of the logarithm is less than the logarithm of the mean. It is shown in appendix B that

$$\overline{\log(W)} = \log(\chi(f) * \bar{W}), \tag{3.4}$$

where

$$0 \leq \chi(f) \equiv \left(\prod_{n=0}^{\infty} (1 - f_n^2)\right)^{1/2} \leq 1 \tag{3.5}$$

is referred to as the "reduction factor." Equation (3.4) can be solved for χ to give

$$\chi(f) = 10^{-\Delta}, \tag{3.6}$$

where

$$\Delta \equiv \log(\bar{W}) - \overline{\log(W)}. \tag{3.7}$$

From (3.5), χ can be determined from f, which in turn is fixed by the standard deviation of $\log(W)$, whereas (3.6) and (3.7) allow χ to be determined from the difference between the log of the mean of W and the mean of the log of W. Small values of W are always difficult to distinguish from the cloud-free zeros, so the mean of $\log(W)$ is more uncertain than the variance. Thus, (3.5) is the preferred way of determining χ. In Fig. 1, $f \approx 0.5$, in which case (3.5) gives $\chi \approx 0.7$. That is consistent with $\bar{W} \approx 92$ g m^{-2}, since $\log(92) \approx 1.96$, which exceeds $\overline{\log(W)}$ by about $\Delta = 0.16$, and $\chi = 10^{-0.16} \approx 0.7$. We shall use this value of χ to make a rough estimate of the albedo bias.

b. *Bias estimate*

The fractal model provides a distribution of W, which can then be converted to optical thickness via (3.1). The computation of the albedo for the fractal model is then a simple matter of determining the reflectivity of each cloud pixel from that pixel's optical thickness, according to the IPA. That requires a table of values supplied by a radiative transfer computation, as discussed in the next section. In order to make a quick estimate of the bias, we consider the highly simplified reflection function given by

$$R(\tau) = \frac{\gamma\tau}{1 + \gamma\tau}, \tag{3.8}$$

where τ is the optical thickness of any particular cloud element, and $\gamma \approx 0.1$. This function is equivalent to one of the two-stream approximations discussed by King and Harshvardhan (1986), and can also be obtained by setting $\theta \approx 45°$ in the analytic form given in Eq. (D1).

From (3.4) and (3.1) we have for the optical thickness

$$\overline{\log(\tau)} = \log(\chi\tau_v), \tag{3.9}$$

since $\bar{\tau} \equiv \tau_v$. If we consider R as a function of $\log(\tau)$, we may perform a Taylor expansion at each pixel about the value of R evaluated at (3.9), so that $R(\log(\tau)) \approx R(\log(\chi\tau_v)) + (\log(\tau) - \log(\chi\tau_v))R' + (\log(\tau) - \log(\chi\tau_v))^2 R''/2 + \ldots$. Averaging this over all pixels eliminates the R' term, and we obtain

$$\bar{R}(\tau_v, f) \approx R(\chi\tau_v) + M_2 R''(\chi\tau_v)/2 + \cdots, \tag{3.10}$$

where $\chi = \chi(f)$ is given by (3.5), $M_2 = M_2(f)$ is the variance of $\log(\tau)$ given by Eq. (B4), and the primes indicate derivatives of R with respect to $\log(\tau)$, evaluated at $\tau = \chi\tau_v$. The next section will explain why the expansion about $\overline{\log(\tau)}$ is preferable to an expansion about $\bar{\tau}$ itself.

If we neglect the derivative terms in (3.10), we see that the mean albedo is simply given by the plane-parallel albedo evaluated at a reduced "effective optical thickness," namely, by

$$\bar{R}(\tau_v, f) \approx R(\chi\tau_v), \tag{3.11}$$

where the reduction factor, χ, is determined from f via (3.5). Harshvardhan and Randall (1985) discussed the concept of a reduced thickness, and estimated a reduction factor of $\chi \approx 1/3$ from global average values of albedo and cloud liquid water. Davis et al. (1990) considered a related quantity, the "packing factor," the inverse of the reduction factor, and showed how it diverges in a singular model, in which case $\chi \to 0$. For parameters appropriate to marine stratocumulus, we find that $\chi \approx 0.7$, obtained by setting $f \approx 0.5$ in (3.5). The next section will show that the derivative terms are small at an intermediate optical depth on the order of $\tau_v \approx 10$ ($\gamma\tau_v \approx 1$), and also that the bias is approximately maximum at these optical depths. We refer to (3.11) as the "effective thickness approximation" (ETA), which is equivalent to the naive rule suggested by Harshardhan and Randall. The ETA is more limited than the IPA, but for the bounded cascade model it gives a good estimate of the maximum bias for medium thickness clouds.

From here on, we adopt the convention that the albedo, as well as the absolute albedo bias, is always expressed as a decimal fraction, while the relative bias will be given as a percent. Then with the approximation (3.11), the relative plane-parallel albedo bias may be expressed as $100*(R(\tau_v) - R(\chi\tau_v))/R(\tau_v)$, since $R(\tau_v)$ equals the plane-parallel albedo, R_{pp}. Substituting (3.8) and setting $\gamma\tau_v = 1$ gives the highly simplified result:

$$\text{relative bias} \approx 100\,\frac{1 - \chi}{1 + \chi}. \tag{3.12}$$

As we have seen from Fig. 1, $f \approx 0.5$ in order to obtained the observed variance of $\log(W)$, and from (3.5) $\chi \approx 0.7$, so according to (3.12) the relative bias is approximately 18%. When the reduction factor is set equal to the global value of $\chi = 1/3$, this bias increases to 50%! This reflects the much greater variance of cloudiness over the globe, as compared to marine stratocumulus variability, which is relatively moderate.

Figure 3 shows graphically how the observed standard deviation of log$W$ (std dev $\approx$ 0.39 for marine stratocumulus) determines the fractal parameter $f \approx 0.5$, which in turn determines the relative plane-parallel albedo bias via Eq. (3.12). The dashed line shows the global estimate. Clearly, observations of the distribution of log$W$ such as those in Fig. 1 need to be extended to other seasons and regions in order to better estimate the associated albedo adjustments like those in Fig. 3, and to understand the effects of cloudiness on the large-scale energy balance.

If realistic amounts of marine stratocumulus liquid water were distributed uniformly over a large ocean basin, then according to (3.12) the large-scale albedo would increase by approximately 18%. We have seen that such a change if made globally would have a large impact on the equilibrium surface temperature. The effect of changing the albedo of marine stratocumulus would be somewhat less dramatic, since they are confined to eastern ocean basins, and would adjust to albedo changes not only through surface temperature, but also by changes in dynamics. Nevertheless, the albedo bias is large enough to be potentially significant, and certainly indicates that the subgrid-scale structure needs to be considered if cloud radiation and cloud liquid water are to be treated consistently.

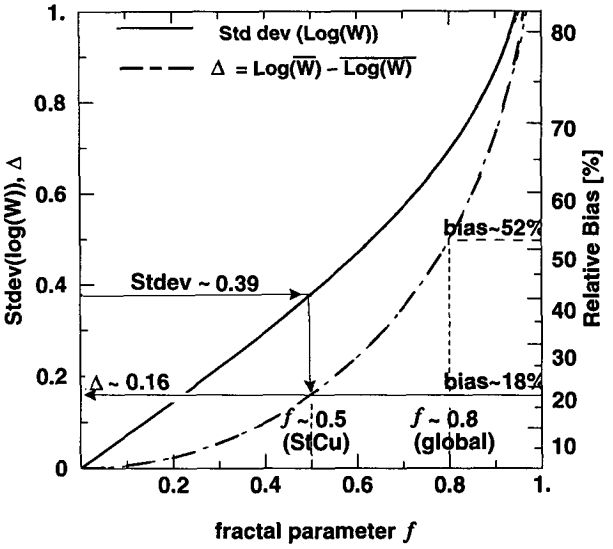

FIG. 3. Plot of the first two logarithmic moments of the bounded model versus fractal parameter f. The solid curve is the standard deviation of the logarithm, and the dashed curve is Δ, the logarithm of the mean minus the mean of the logarithm. Both curves are plotted on the left-hand vertical axis. Base 10 logarithms are used, and the curves apply equally to the vertical optical thickness or the liquid water path because of Eq. (3.1). The Δ determines the reduction factor χ by Eq. (3.6), and thus the relative albedo bias by (3.12), so that the dashed curve also determines the bias, plotted on the rescaled right-hand vertical axis. The lower horizontal lines indicate graphically how the observed value of Stdev(log$W$) is used to determine $f \approx 0.5$, which in turn gives a rough estimate of the plane-parallel albedo bias of $\Delta R_{pp}/R_{pp} \approx 18\%$. Similarly, the upper horizontal lines show that the global estimate of $\chi \approx 1/3$ corresponds to a bias of about 50%, and to $f \approx 0.8$, giving a global value of std dev(log$W$) ≈ 0.7.

4. Conservative scattering

This section applies the IPA to compute the area-average albedo of cloudiness generated by the bounded cascade model described in section 3, using an analytic reflection function for conservative scattering which generalizes Eq. (3.8), as well as a numerical reflection function computed from the fair weather cumulus (FWC) phase function of King and Harshvardhan (1986). A discussion of the properties of the reflection function, $R(\tau, \theta)$, will be followed by a discussion of the plane-parallel bias, $\Delta R_{pp}(\tau_v, \theta, f)$. The dependence of the bias on the optical thickness, sun angle, and fractal parameter will be made clear, as well as the advantage of expressing the bias in terms of moments of $\log(W)$, or equivalently $\log(\tau)$, as in Eqs. (3.9) and (3.10), rather than W or τ.

a. *Properties of the reflection function*

The upper curve in Fig. 4a shows the analytic reflection function discussed in appendix D, Eq. (D1), plotted as a function of the vertical optical thickness for a sun angle of 60°. It rises linearly from zero with a slope given by the backscatter fraction and reaches a value of 0.69 at $W = 100$ g m^{-2}, or equivalently $\tau_v = 15$. The lower curves in Fig. 4a show the area-averaged reflectivity for increasing values of the fractal parameter, $f = 0.25, 0.5, 0.75$, as computed by expanding the reflectivity of each pixel as in (3.10). The $f = 0.5$ curve, typical of FIRE as indicated in Fig. 1, reaches a value of 0.60 at $W = 100$ g m^{-2}, or $\tau_v = 15$.

The fact that the mean albedo decreases as f increases for any given mean optical thickness is a result of the convexity of R. As the distribution of τ widens, the *darkening* of those pixels where the optical depth decreases by a given amount *exceeds the brightening* of those pixels where the optical depth increases by the same amount, so that the average cloud brightness decreases. As a result, the plane-parallel albedo bias is strictly positive. This is an example of "Jensen's inequality" (Jensen 1906). This inequality holds only in the context of the IPA. Errors in the IPA can be of either sign, due to effects of horizontal photon transport.

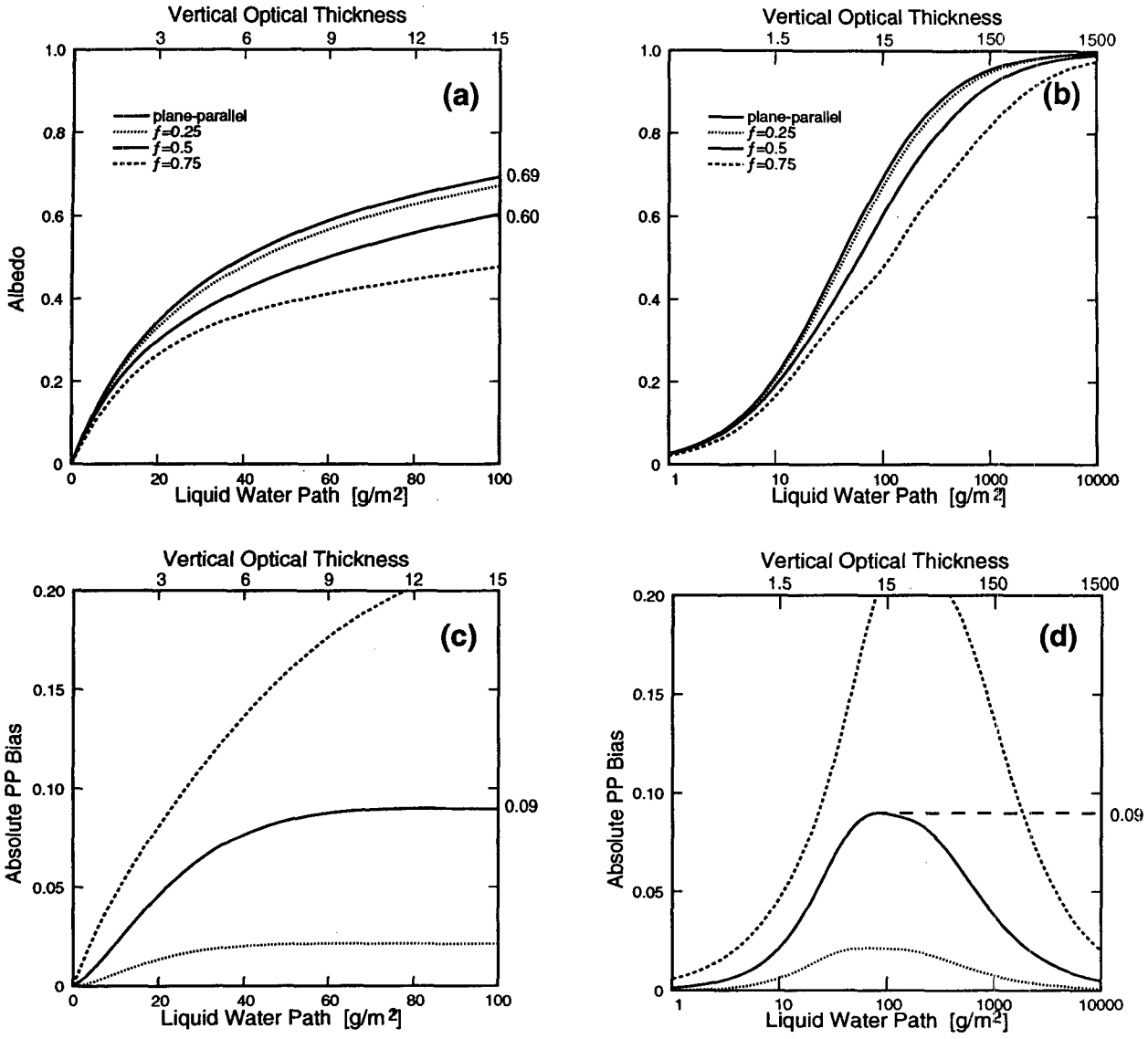

FIG. 4. (a) Area-averaged albedo with the sun at 60° versus W, with the equivalent τ_v shown on the upper horizontal axis. The upper curve shows the plane-parallel albedo, which rises to 0.69 at $W = 100$ g m^{-2}. The lower curves show the bounded model albedos for $f = 0.25$, 0.5, and 0.75, which rise to 0.67, 0.60, and 0.51, respectively. Subtracting the lower curves from the upper one gives the absolute plane-parallel bias, which, for example, equals 0.09 at $W = 100$ when $f = 0.5$. The sign of the bias is related to the convexity of these curves, as explained in the text. (b) The same curves as in (a) are plotted here out to $W = 10\,000$ on a log scale. The change in the sign of the curvature that occurs at intermediate values leads to the simplified "effective thickness approximation" (ETA) expressed in (3.11). (c) The bias is plotted for the same three values of f over the same range of W as in (a), showing that the bias is approximately constant over the observed range of W. (d) The bias is plotted here on the same $\log(W)$ scale as in (b), showing that it eventually returns to zero.

b. *Dependence of the bias on optical thickness*

Subtracting each of these lower curves in Fig. 4a from the upper plane-parallel curve gives the absolute plane-parallel bias plotted in Fig. 4c, and computed analytically as

$$\overline{\Delta R_{pp}}(\tau_v, \theta, f) = R(\tau_v, \theta) - \{R(\tau_{\text{eff}}, \theta) + M_2 R''(\tau_{\text{eff}}, \theta)/2\}, \quad (4.1)$$

where the primes indicate derivatives of the reflection function with respect to $\log(\tau)$, evaluated at the reduced effective optical thickness given by

$$\tau_{\text{eff}} \equiv \chi \tau_v, \quad (4.2)$$

with the reduction factor χ defined in (3.5). Equation (4.1) is derived in the same way as (3.10), by expanding the pixel reflectivities about $\overline{\log(\tau)}$, area averaging, and subtracting the result from the plane-parallel reflectivity.

The vanishing of the bias for thin clouds is a consequence of the linearity of the reflection function for small τ_v, since in that case the mean reflectivity equals the reflectivity of the mean. For clouds of intermediate thickness, $6 \leq \tau_v \leq 30$, the bias is relatively insensitive to the mean vertical optical thickness. In Fig. 4d the bias is plotted versus $\log(\tau_v)$, to show that for extremely thick clouds, $\tau_v \geq 100$, the bias eventually returns to zero, since for the bounded model even the thinnest pixel eventually becomes 100% reflective. (Stratocumulus cloud optical depths of 100 are, of course, of only theoretical interest, although in highly absorptive clouds the bias becomes sensitive to the mean at more accessible values, as discussed in section 5.) For the fractal scale parameter used here, namely, $c \approx 0.8$, the maximum bias occurs in the observed range of thicknesses seen in FIRE. For larger c, however (i.e., for a flatter spectrum), this maximum moves to larger τ_v until for the singular model, $c = 1$, it is only reached in the infinitely thick limit.

The convexity of the reflection function seen in Fig. 4a means that the second derivative, or curvature, of the reflection function is negative. When plotted on a logarithmic scale like that of Fig. 4b, however, the curvature becomes positive for thin clouds, vanishes at some intermediate thickness, and is negative for thick clouds. The coefficient of the M_2 term in the analytic bias expression in Eq. (4.1) is exactly the logarithmic curvature of R, so that this term becomes small at intermediate τ_v, near the inflection point of Fig. 4b, which is also the region for which the bias is approximately maximum. For this intermediate thickness, then, we may keep only the first term in curly braces in (4.1), implying that the mean reflectivity is approximately equal to the plane-parallel reflectivity evaluated at the reduced effective thickness τ_{eff}, as in the ETA of (3.11). Thus, the ETA gives a good estimate of the bias for clouds of intermediate thickness in the vicinity of the maximum of the bias curve in Fig. 4d.

As Harshvardhan and Randall (1985) commented, on a global scale it is necessary to reduce the observed values of $\bar{W}$ or τ_v by a factor of 1/3 in order to obtain a reasonable albedo from a plane-parallel model. Stephens (1985) replied that this "fudge factor" is not likely to be a universal constant, but must depend upon statistical information about the distribution of W. That is exactly the information expressed by $\chi(f)$ for clouds having a $k^{-5/3}$ wavenumber spectrum and a lognormal-like PDF. As we have seen, setting $\chi = 1/3$ in (3.12) gives a 50% relative bias, which from Fig. 3 corresponds to $f \approx 0.8$, or $\Delta \approx 0.5$ and std dev(log) ≈ 0.7. As shown in the next subsection, this rough global estimate should actually be reduced for stratocumulus to about 15%. The much greater variability and albedo bias required by the global estimate, as compared to the marine stratocumulus case, is related to the much wider variability of clouds on the global scale. One example is the contribution of deep convection to the global albedo. A better understanding of radiative transfer in deep convection will require observations of liquid water in tropical cloud clusters with sufficient spatial and temporal sampling to extract statistical properties analogous to the stratocumulus liquid water distribution shown in Fig. 1. It will also require the development of fractal models appropriate to each particular cloud type and meteorological regime.

Since the analytic expression (4.1) is clearly useful in understanding the albedo bias, it is important to assess its accuracy. Here that will be done with IPA computations. The accuracy of the IPA has itself been verified by Monte Carlo calculations, as reported separately (Cahalan et al. 1994). Since the plane-parallel reflectivity is a smooth function, accurate IPA estimates may be computed from a detailed numerical table, from which the reflectivity for any given value of θ and τ may be interpolated. The solid curve in Fig. 5 shows the *relative* albedo bias computed from such a "lookup table" computation, using a table computed from the FWC phase function of King and Harshvardhan (1986), and the same parameter values used for the

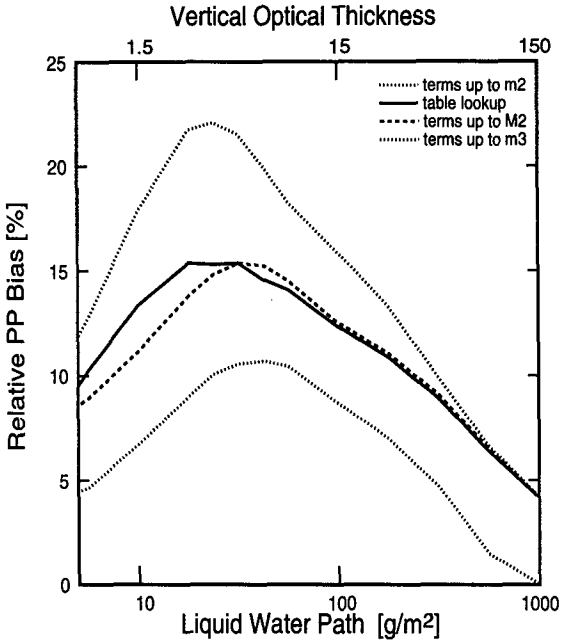

FIG. 5. The relative "plane-parallel bias," namely, the absolute plane-parallel bias divided by the plane-parallel albedo. The solid line is computed from the middle curve ($f = 0.5$) in Fig. 4d. It reaches a maximum at optical thickness $\tau_v = 6$ of about $100*0.075/0.5 = 15\%$. This peak value is slightly less than the estimate made from Eq. (3.12) in the text. The upper dotted curve is an overestimate based only on the variance of W, neglecting the skewness of the distribution, while the lower dotted curve gives an underestimate that includes the skewness but neglects the fourth moment. This expansion in moments of W alternates sign and converges slowly. An expansion in moments of $\log W$ converges from below since there are only even moments, and much more rapidly, as shown by the dashed curve, which includes only moments up to the variance of $\log W$.

solid curve in Fig. 4d. Note that the relative bias rises to its maximum of about 15% more rapidly than the absolute bias, nearly reaching it by $\tau_v = 1.5$. The dashed curve shows the analytic expression for the relative bias obtained by dividing (4.1) by the plane-parallel reflectivity. It approximates the numerical results over the range of interest, $\bar{W} \geq 10$ g m^{-2}, or $\tau_v \geq 1.5$, to better than 1%. [Note that the analytic estimate relies mainly on the accuracy of the logarithmic curvature of R, rather than R itself. Differences between the FWC table and the analytic R of appendix D are in fact somewhat larger, and reach a maximum of about 10% near $\theta \approx 45°$, remaining less than 5% elsewhere except near the horizon.]

The two dotted curves in Fig. 5 come from an expression similar to (4.1) but are obtained by expanding the pixel reflectivities about $\bar{W}$, or τ_v, rather than $\overline{\log\tau}$, and then averaging, keeping moments up to the variance (upper curve) or the skewness (lower curve). Clearly, the expansion about $\overline{\log\tau}$ as in (4.1) provides a much better approximation than an expansion about $\bar{\tau}$. This occurs because the log expansion has two advantages: 1) the distribution is symmetric about the mean logarithm, so the logarithmic skewness and all other odd logarithmic moments vanish, giving more rapid convergence; 2) the derivative coefficients in the expansion in linear moments alternate in sign, giving first an overestimate, then an underestimate, etc., as shown by the dotted curves in Fig. 5, while as we have seen, the logarithmic curvature and higher derivatives tend to be small where the bias is large.

c. *Dependence of the bias on sun angle*

The above results were restricted to a solar zenith angle of 60°, typical of the FIRE observations. Figures 6a and 6b show contour plots of the absolute and relative plane-parallel albedo bias, respectively, as a function of both optical thickness and the cosine of the solar zenith angle, as computed from the same FWC reflectivity table used in Fig. 5. (Similar results have been obtained with the Henyey–Greenstein phase function.) As seen in Fig. 6a, at a mean vertical optical thickness of $\tau_v \approx 15$ the bias is less than 0.04 near the horizon; it increases to 0.08 near $\theta = 60°$, corresponding to the peak in Fig. 4c, and then to 0.1 near the zenith.

For sun angles within 30° of the zenith (i.e., $\cos\theta \geq 0.5$), the bias decreases away from the zenith, with the absolute bias peaking near $\tau_v \approx 15$–30 and the relative bias peaking near $\tau_v \approx 5$–10. Intuitively, the bias decreases as the sun gets lower because the variable cloud looks more uniform away from the zenith, since the reflection of each pixel is larger. However, this naive argument fails for thin clouds, as the plots show. For example, at $\tau_v \approx 1$, the bias is still small near the horizon, but increases to a maximum when the sun is only about 15° above the horizon, and then decreases toward the zenith. The variability of very thin clouds is more significant at larger solar zenith angles.

d. *Dependence of the bias on fractal parameter f*

The absolute albedo bias was estimated above to be about 0.09, and the relative albedo bias about 15%, based on a value of the fractal parameter typical of the FIRE stratocumulus observations, $f \approx 0.5$. We saw above, however, that a value closer to $f \approx 0.8$ is needed for global estimates, and in section 6 we shall consider values down to $f \approx 0.3$ during the diurnal cycle of stratocumulus. The reduction factor computed from (3.5) for $f = 0.3$, 0.5, and 0.8 is roughly $\chi = 0.9$, 0.7, and 0.3, respectively, resulting in a relative bias of approximately 5%, 18%, and 54%, respectively, as estimated from Eq. (3.12).

These naive estimates from (3.12) clearly indicate that the albedo bias increases rapidly with the fractal parameter. That is verified by more detailed "lookup table" computations using the FWC table, as shown by Fig. 7, which is a contour plot of the relative bias as a function of f and τ_v, for $\theta = 60°$. The maximum bias values at $f = 0.3$, 0.5, and 0.8 are 5%, 15%, and 38%, respectively. The bias varies very little with the mean optical thickness, remaining nearly equal to its maximum value over the range $1 \leq \tau_v \leq 100$. (Similar results have been obtained with the Henyey–Greenstein phase function.)

5. Absorption

In order to assess the effects of absorption on the plane-parallel albedo bias, the same "table lookup" approach was applied to compute the mean reflectivity of stratocumulus clouds generated by the bounded cascade model, for values of the single scattering albedo less than unity. The resulting relative bias is shown in Fig. 7b for a single scattering albedo of $\omega_0 = 0.99$. Comparing this to the conservative case, Fig. 7a, it is evident that the maximum relative biases in both cases at, say, $f = 0.3$, 0.5, and 0.8 are still approximately equal to the conservative values of 5%, 15%, and 38%, but now these occur at somewhat lower values of τ_v, and the bias decreases more rapidly for thick clouds. For example, at $f = 0.5$, the bias still exceeds 5% at $\tau_v = 100$ in the conservative case, but is about 1% at when $\omega_0 = 0.99$. It falls well below 1% at $\tau_v = 100$ in the extreme case of $\omega_0 = 0.90$ (not shown).

The bias is most sensitive to changes in the mean optical thickness where the derivative with respect to τ_v is maximum. We have seen from Fig. 4d that the bias becomes sensitive to the mean only at thicknesses ~ 100 when $\omega_0 = 1.0$ and $f = 0.5$, whereas Fig. 7b shows that the bias becomes sensitive to the mean already at thicknesses ≈ 80 when $\omega_0 = 0.99$ and $f = 0.5$. Even in the strongly absorptive case this occurs well above the mean thicknesses seen in marine stratocumulus.

These results indicate that plane-parallel computations are likely to be quite good for thick strongly ab-

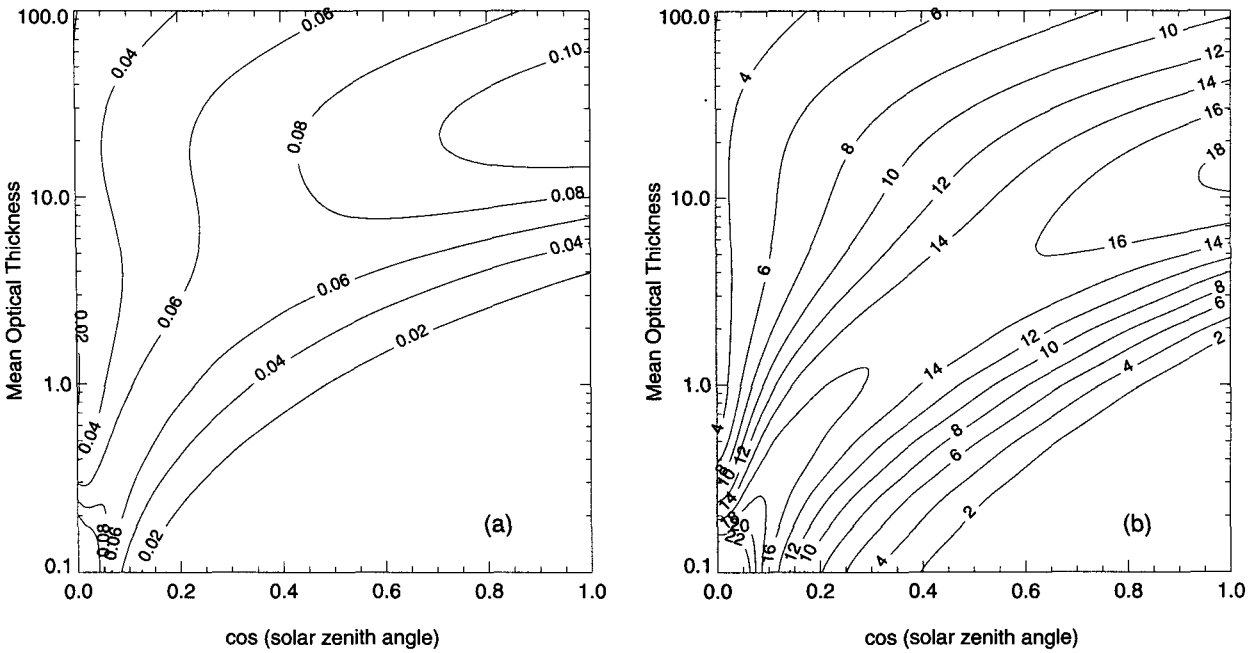

FIG. 6. (a) The absolute plane-parallel albedo bias for the bounded model with $f = 0.5$, $c = 0.8$, and $\omega_0 = 1.0$, defined as in Fig. 4, but as a function of sun angle and mean vertical optical thickness. (b) The relative plane-parallel albedo bias with the parameters as in (a), and defined as in Fig. 5.

sorbing clouds. Of course, such clouds generally have a much smaller albedo than nonabsorptive clouds, and thus have less impact on the planetary average albedo over dark ocean surfaces. Note that such strongly absorbing clouds cool the surface independent of the surface albedo, due to the low transmission of solar en-

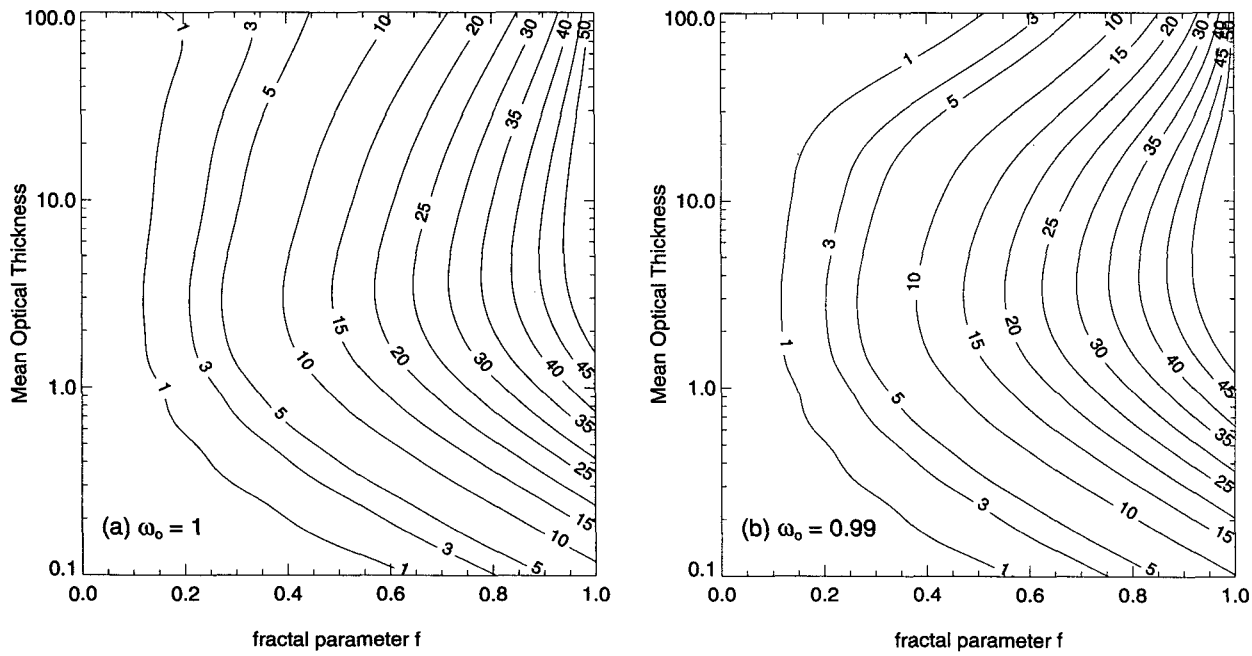

FIG. 7. The relative plane-parallel albedo bias for the bounded model with $f = 0.5$, $c = 0.8$, and for (a) $\omega_0 = 1.0$ and (b) $\omega_0 = 0.99$, defined as in Fig. 5 but as a function of fractal parameter and mean vertical optical thickness.

ergy. An extreme example of this was the cloud formed from the soot plumes of the 1991 Kuwait oil fires, which had a single scattering albedo on the order of 0.6 and lowered surface temperatures under the plumes by 10°C [see, for example, Cahalan (1992) and other papers in that issue].

6. Stratocumulus diurnal cycle

Since the fractal parameter, f, is determined by the variance of $\log W$, it is interesting to examine the diurnal change in f implied by observed changes in the variance of $\log(W)$. By compositing the 1-minute-averaged values of W over the 18 days used to determine Fig. 1, for each hour of the day, we can determine the mean and variance of W over the full diurnal cycle for California marine stratocumulus during July 1987. As in Fig. 1, only measurements exceeding 10 g m^{-2} are included, and the fraction above this threshold defines the cloud fraction, which is thus also known for each hour.

Results of this analysis are shown in Fig. 8, which shows the diurnal variations of the mean vertical optical thickness $\tau_v = W/0.15$, the solar zenith angle in degrees at San Nicolas Island during July, the cloud fraction, and the fractal parameter f. The optical thickness has an early morning maximum of $\tau_v = 24$ around 0600 local time and a secondary maximum around 0900 then falls to a minimum of $\tau_v = 6$ in the late afternoon. This is the least important of the plots, since the albedo bias is relatively insensitive to changes in τ_v over this range, as was seen in Figs. 4 and 7. The average cosine of the sun angle is 0.54, corresponding to 57°. The cloud fraction reaches a maximum near 100% at 1100, and drops to about 60% at 1600. During the morning hours, when the cloud fraction is high, the within-cloud variability is also high, with f reaching a maximum of about 0.6, while in the afternoon f decreases to about 0.3, the average being 0.46. Corrections made to the cloud albedo in climate models usually depend only on the cloud fraction and solar zenith angle, and in this case would only be important in the afternoon when the cloud fraction is low and the sun is high. We will now show, however, that the most significant correction to the plane-parallel albedo of stratocumulus occurs in the morning, when the variability is large, so that the fractal parameter is nearly maximum, despite the fact that the cloud fraction is also nearly maximum at that time.

To estimate the albedo bias for nonovercast situations, we need a model for the clear sky reflectivity, and we shall assume that it vanishes for all zenith angles. Thus, we assume that the ocean is perfectly absorbing, so that the albedo is zero. We also ignore haze, small cumulus clouds, and other atmospheric effects that are especially important when the sun is near the horizon. This error makes little difference at sunrise, when the cloud fraction is nearly 100%. But our results become untrustworthy in the late afternoon and evening, when the sun begins to set, and the clear fraction still exceeds 30%. With this caveat, the parameters of Fig. 8 were used as input to an IPA computation of the absolute plane-parallel albedo bias, and the results are shown in Fig. 9. The solid line, which shows the total bias, reaches a maximum of about 0.10 around 0900–1000 when the cloud coverage is nearly overcast, then falls to a minimum of about 0.06 at 1500, before increasing again due to the "limb bias" caused by our neglect of the clear sky reflectance.

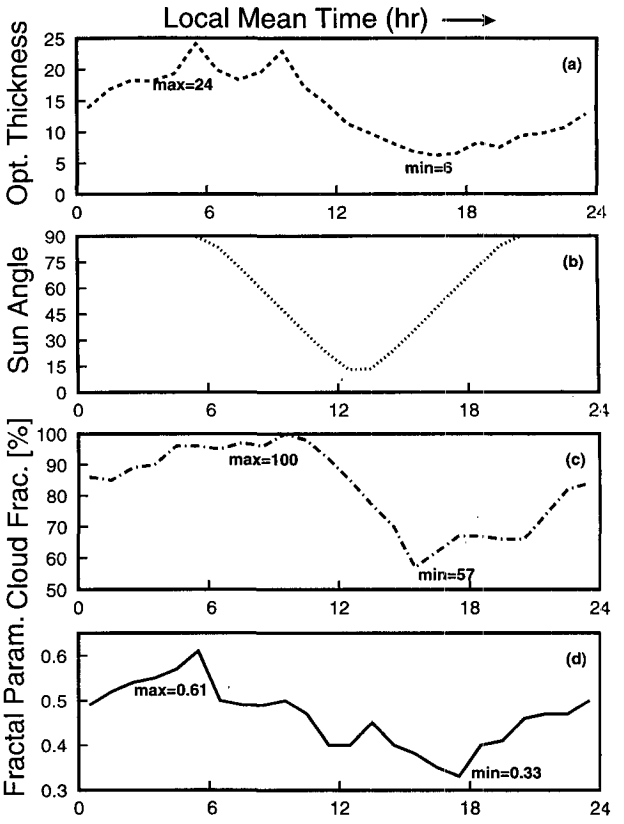

FIG. 8. Diurnal variations in (a) mean vertical optical thickness [from W via (3.1)]; (b) solar zenith angle (for San Nicolas Island in July); (c) stratocumulus cloud fraction (from fraction with $W > 10$ g m^{-2}); and (d) fractal parameter (from std dev($\log W$) via Fig. 3). All cloud parameters are determined by compositing histograms like that in Fig. 1 for each hour of the day during the 18-day 1987 FIRE period.

To better understand the total absolute bias, we can split it into two parts as follows:

$$\Delta R_{pp}(A_c, f) = [R_{pp}(100\%) - R_{pp}(A_c)] + [R_{pp}(A_c) - R_f(A_c)]. \quad (6.1)$$

Here the total bias is the difference between the first and last terms, where the first term is computed with the cloud liquid water uniformly covering 100% of the region, and the last term is computed from a fractal distribution of the same amount of total liquid over the

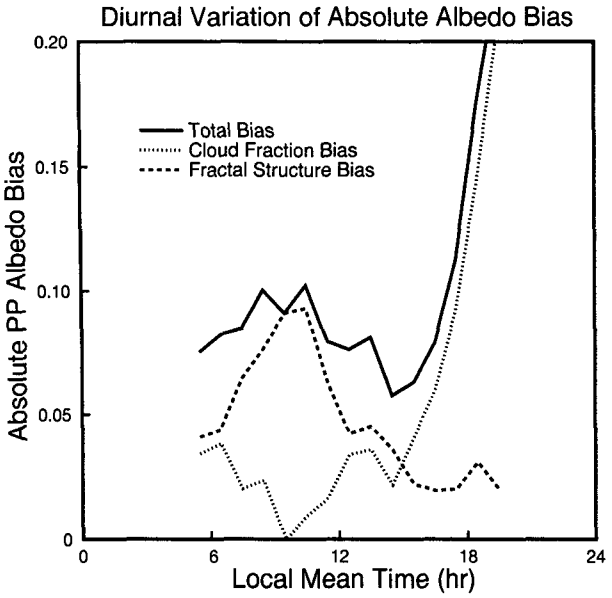

FIG. 9. Diurnal variation of the absolute plane-parallel albedo bias for stratocumulus clouds, computed from the diurnal variations in cloud properties shown in Fig. 8. The dotted curve is the contribution due only to the cloud fraction, using only plane-parallel computations. The dashed curve is the additional bias associated with the within-cloud variability. The sum of the dotted and dashed curves equals the total bias given by the solid curve, as in Eq. (6.1).

cloud fraction A_c. The contribution of the cloud fraction can be separated from that of the within-cloud fractal structure by summing the bias due to changing only A_c, without changing the uniform distribution, to the bias computed by keeping A_c fixed, and replacing the uniform distribution by the bounded cascade.

It is clear that the relative importance of the fractal structure must increase with cloud fraction, independent of the bounded cascade model, since the first term in (6.1) vanishes as $A_c \rightarrow 100\%$. The increase in importance of within-cloud structure with A_c is enhanced by the observed fact that the within-cloud variance is greatest in the morning when $A_c \rightarrow 100\%$, resulting in the larger values of f in Fig. 8 during the morning hours.

The first difference in Eq. (6.1), the "cloud fraction bias," is plotted as the dotted line in Fig. 9. It falls to zero in the morning when the cloud fraction reaches 100% and then rises as the sun goes down to a value equal to the cloud fraction, due to the limb bias. The second difference, the "fractal structure bias," is initially roughly equal to the cloud fraction bias at sunup but then rises to dominate the total bias in late morning, before decreasing to less than 0.05 again in the afternoon.

Because of the high variability in the cloud structure during the morning hours, the plane-parallel approximation for cloud albedo tends to be most in error in the morning, precisely when the cloud fraction is approaching 100%! The usual albedo correction due to cloud fraction is small, and also out of phase with the total bias. Thus, in estimating the stratocumulus cloud albedo, the cloud fraction is not only less important than the within-cloud variability, but also misleading in its dependence on local time, at least for the California stratocumulus clouds seen during 1987 in FIRE.

7. Results and discussion

In plane-parallel theory, the horizontal-average reflectivity is computed from the horizontal-average vertical optical thickness. But the average reflectivity and other mean radiative quantities are also sensitive to the *variance* of the cloud optical thickness. A given amount of total cloud liquid water invariably produces the greatest mean albedo when it is uniformly distributed as in the plane-parallel model, so that plane-parallel estimates have a positive "plane-parallel albedo bias." Current GCMs attempt to parameterize the albedo bias in terms of the "cloud fraction," but for marine stratocumulus, a major contributor to net cloud radiative forcing, the *within-cloud* variance is responsible for most of the plane-parallel albedo bias, while the bias contributed by the cloud fraction vanishes precisely when the bias is largest. (In the bounded cascade model, the within-cloud variance is determined by the fractal parameter f, while the distribution of variance with wavenumber, i.e., the spectrum, is determined by the scaling parameter c.) The within-cloud variance has a diurnal variation, as discussed in section 6, and presumably also an annual variation, which is not yet known. Hopefully, future field experiments will provide more climatological information about this fundamental quantity, both for the various stratocumulus regimes and for the other cloud types and meteorological conditions that make significant contributions to the large-scale climate.

The main results of this study are summarized as follows:

1) An inhomogeneous cloud field has a lower mesoscale-average albedo than a plane-parallel cloud having the same microphysical structure and the same total liquid water. Thus, a given cloud field has a positive *plane-parallel albedo bias* for any given fractal structure.

2) The mesoscale-average albedo of the FIRE marine stratocumulus clouds is more sensitive to the within-cloud fractal structure than it is to the cloud fraction. The albedo bias due to the within-cloud structure is largest for overcast clouds for any given fractal structure.

3) Plane-parallel estimates of the mesoscale-average albedo of the FIRE marine stratocumulus are most in error when the cloud variability is largest, which occurs when the cloud fraction is largest, when the cloud optical thickness is moderate (≈ 10), and when

TABLE 1. Primary quantities and symbols.

Quantity	Symbol	Typical values
	Fractal cascade	
Variance parameter	f	0.5 (0.8 global)
Spectral parameter	c	0.8 ($k^{-5/3}$ spectrum)
Reduction factor	χ	0.7 (0.3 global)
	Macrophysical	
Integrated liquid water	W	90 g/m^2
Mean vertical optical thickness	τ_v	15
Reduced vertical optical thickness	τ_{eff}	10
Pixel vertical optical thickness	τ	0.1–100
Sun angles	θ, ϕ	60°, 0°
	Microphysical	
Asymmetry parameter	g	0.843
Single scattering albedo	ω_0	0.99–1.0
	Cloud/solar flux ratios	
Reflected, transmitted, absorbed	R, T, A	0.6, 0.4, 0.0
Independent pixel (ip) estimates	R_{ip}, T_{ip}, A_{ip}	0.6, 0.4, 0.0
Plane-parallel (pp) estimates	R_{pp}, T_{pp}, A_{pp}	0.7, 0.3, 0.0
pp biases ($R_{pp} - R_{ip}$, etc.)	$\Delta R_{pp}, \Delta T_{pp}, \Delta A_{pp}$	0.1, −0.1, 0.0
ip biases ($R_{ip} - R$, etc.)	$\Delta R_{ip}, \Delta T_{ip}, \Delta A_{ip}$	0.0, 0.0, 0.0

the sun is nearest to the zenith. The absolute bias is typically about 0.09 and the relative bias is about 15%. (For thin clouds of optical thickness ~1, the maximum bias occurs when the sun is near the horizon.)

4) For the FIRE marine stratocumulus, the albedo can be estimated from the plane-parallel albedo for an "effective" vertical optical thickness that is reduced from the mesoscale-averaged value by a factor $\chi \approx 0.7$. This "effective thickness approximation" (ETA) is most accurate at intermediate thicknesses (≈ 10). The reduction factor χ varies with local time and presumably with season and region.

The FIRE observations on which these estimates are based were affected by their proximity to land and show somewhat higher mean values than farther offshore (Minnis et al. 1992). However, the albedo bias mainly depends on the variance and wavenumber spectrum of the cloud liquid, and not the mean. The spectral exponent agrees with those observed for other scalar quantities over a wide range of scale (e.g., Gage and Nastrom 1986). The variance of the logarithm of the integrated liquid water has not yet been widely observed. As we have seen, it is a fundamental parameter for determining inhomogeneous corrections to plane-parallel albedo estimates, on the same level of importance as the cloud fraction. It is crucial that a climatology of this quantity be compiled, at least for marine stratocumulus clouds, which are essential to the net cloud radiative forcing.

Large errors in regional quantities such as surface temperature and/or heat fluxes to other regions, which would result from a 15% plane-parallel albedo bias, are avoided by current climate models either by adjusting the albedo directly, thus decoupling cloud liquid from cloud radiation, or reducing the cloud liquid. If such a "reduction factor" can in fact be sensibly defined, it must depend upon the fractal structure, as exemplified here by $\chi(f)$, defined in Eqs. (3.4)–(3.7). In the bounded cascade model, the "effective thickness approximation" for the mesoscale-average albedo can be justified for optical thicknesses typical of marine stratocumulus. The reduction factor $\chi(f)$ is a function of the fractal parameter, and according to the FIRE observations is about 0.7. Thus, the typical observed value of 90 g m^{-2} (see Fig. 1) is reduced to 63 g m^{-2}, corresponding to a reduction in optical thickness from 15

TABLE 2. Comparison of cascade models.

Quantity	Singular model	Bounded model
Cascade fractions	$f_n = \text{const} = f$	$f_n = f * c^n$, $c \approx 0.8$
Maximum thickness	$\tau_{\max} \to \infty$	$\tau_{\max} < \tau_v \exp(f/(1-c))$
Wavenumber spectrum	$S(k) \sim k^{-1}$ or flatter	$S(k) \sim k^{-5/3}$
Plane-parallel bias	>20%	15%
IPA bias	<−10%	≤1%

to 10, and a corresponding reduction in albedo from 0.69 to 0.60. Harshvardhan and Randall found that a much more dramatic reduction in global cloud liquid, by a factor of $\chi(f) \approx 0.3$, is needed to obtain a reasonable global albedo. The bounded model is not generally appropriate for other cloud types that contribute to the global albedo. Other cloud types are likely to have larger albedo biases, but careful estimates must await the development of more appropriate models.

Our conclusions rely upon three main simplifying assumptions:

1) independent pixel approximation (IPA);
2) constant droplet radius ($\tau_v = 0.15W$);
3) bounded cascade model ($f_n = fc^n$).

We now discuss each of these in turn.

The most significant of these assumptions is the IPA, which has been thoroughly tested for both the bounded cascade model and the singular model, as reported in a separate paper (Cahalan et al. 1994). As shown there, the IPA is quite accurate for the bounded model due to the rapid falloff of the wavenumber spectrum. While the accuracy of the IPA depends on the spatial pattern, the IPA results themselves depend only on the one-point probability distribution function shown in Fig. 1 and not on how the liquid is distributed spatially: whether in streets as in Fig. 2 or in a more general two-dimensional pattern. Even in the singular model, where the IPA errors are large, the simplicity of the IPA makes it a convenient tool for exploring the parameter space to determine where more detailed and expensive Monte Carlo computations are likely to be necessary.

Although the IPA has sometimes been loosely referred to as a "plane-parallel computation," it depends on all the moments of the one-point PDF, including both the mean and the variance, so that it is important to distinguish it from a simple plane-parallel computation, which is strictly a function of the mean quantities. Of course each individual pixel contribution to the IPA *is* a simple plane-parallel computation and has its own associated plane-parallel bias, due to the neglected subresolution variability and also due to radiation from neighboring pixels. In a separate paper (Cahalan et al. 1994), we show that these individual biases can be quite large but tend to cancel out in the area average when the variability is generated by a bounded cascade. While we have focused here purely on the *mesoscale-average* albedo relevant to climate models, an important alternative application is the determination of errors in remote sensing estimates of cloud properties, such as the ISCCP estimates of cloud optical thickness (Rossow and Schiffer 1991). Cloud optical thickness estimates determined from 1-km satellite pixels tend to be smaller than those found by in situ observations. One source of such discrepancies may be a "reduction factor" due to subpixel inhomogeneity.

There is evidence that the droplet radius varies with optical depth in opposite directions for thick and thin stratocumulus clouds, as discussed, for example, by Nakajima et al. (1991). There is also some evidence that r_{eff} may depend upon the fractal cloud structure, since there is some evidence that drop sizes are smaller near cloud perimeters (Durkee 1988; Minaert 1988; Coakley 1991; Wielicki and Parker 1992), so that the area-average r_{eff} may depend on the perimeter fractal dimension. Our goal in the present paper has been to estimate the albedo bias for clouds that have the observed wavenumber spectrum and probability distribution observed for stratocumulus liquid water, while being otherwise as nearly plane parallel as possible. In that spirit, we have neglected variations in both the cloud microphysics and the cloud shape. More observations and theoretical work are needed in order to better understand the correlations between cloud microphysics and cloud geometry.

The bounded cascade model used here generates a continuous distribution of liquid water and optical depths, bounded both above and below. The distribution becomes spatially uniform at small scales, and has the observed $k^{-5/3}$ wavenumber spectrum. It is a very conservative substitute for the plane-parallel model. Thus, the estimates for the plane-parallel albedo bias given here are also conservative.

Note that the first two results listed above, namely, the positivity of the bias and the increase of the bias with cloud fraction, do not depend on the specific structure of the bounded cascade model pictured in Fig. 2. They follow more generally from the IPA, which relies mainly on the observed rapid falloff of the wavenumber spectrum of cloud liquid water and the low-order moments of the PDF.

The bounded cascade is perhaps the simplest model that is able to reproduce both the power-law wavenumber spectrum and the lognormal-like PDF shown in Fig. 1. Additive models, such as a simple Fourier series, generate normally distributed cloud liquid values, thus omitting the skewness, which makes a large contribution to the bias as shown in Fig. 5. On the other hand, a purely lognormal PDF distributed randomly in space omits the observed spatial correlations, which make the IPA applicable to stratocumulus clouds. The distribution generated by the bounded cascade is simpler and more realistic than a lognormal because of its bounded character.

More complex cascade models must reproduce the observed PDF and wavenumber spectrum of the vertically integrated liquid water, as the bounded cascade does, but they may also attempt to simulate the vertical cloud structure. The present study of the effects of horizontal inhomogeneity is complemented by that of Stephens et al. (1991), which considered a horizontally uniform cloud layer having a random distribution of optical depth in the vertical direction. (Variations in single-scattering albedo were found to be less significant.) In marine stratocumulus, the mean quantities increase linearly with height, so that most of the liquid

water is concentrated within a few tens of meters near the cloud top, which is where most of the reflection occurs. Monte Carlo studies show that the photon field tends to smooth out variations on the order of the photon mean free path of about 100 m (Cahalan 1989), so that smaller-scale variations do not alter the average albedo. Thus, we doubt that the vertical variations in marine stratocumulus liquid water would affect our estimates of the average albedo. However, further development of cascade models to include both horizontal and vertical variations is certainly needed, and must be accompanied by observations of both vertical and horizontal variability.

The 15% reduction in reflectivity found here due only to liquid water variability, with no change in mean liquid water or cloud fraction, is as large as that found by Coakley (1991) due to increased "brokenness," as inferred from the spatial coherence method applied to 1-km AVHRR satellite data. Such variability in satellite-observed reflectivity is commonly interpreted in terms of cloud fraction, but may also arise from varying liquid water amounts, as well as other inhomogeneities in the cloud field. Although this paper has focused upon the mesoscale biases appropriate for climate models, error estimates on the 1-km scale appropriate for remote sensing must also rely upon models of cloud structure that reproduce the observed dependence of cloud variability on spatial scale, cloud type, season, and local time.

Larger plane-parallel albedo biases are expected for other cloud types, such as cirrus or deep cumulus, that exhibit structures much further from being plane-parallel than stratocumulus. Errors in plane-parallel estimates of mesoscale-average emissivity of such clouds may partially compensate the albedo bias, perhaps leading to a smaller bias in *net* fluxes. The fractal statistics of such clouds, however, are still poorly known. Other cloud types not only exhibit a much broader distribution of liquid water, but also are much more spatially complex. Computing the larger radiative biases for such clouds, in both the solar and thermal regimes, will require considerable observational data, more subtle fractal models, and highly optimized three-dimensional Monte Carlo radiative transfer codes. Some of the observations will come from the Atmospheric Radiation Measurement (ARM) field program. As that occurs, the fractal models will need to be made more realistic and will gradually become more constrained by the data. Realistic radiative computations need to be tied to the attempts now under way to incorporate the hydrological cycle into global climate models, so that the cloud liquid water and the cloud radiation will eventually be treated consistently.

Acknowledgments. We are grateful to Harshvardhan and G. L. Stephens for helpful discussions on the albedo bias, to M. King for use of his FWC phase function results, and to W. Rossow for several helpful comments. This work would not have been possible without the assistance of D. Silberstein, who is responsible for a number of the graphs and associated computations. Support from NASA Contracts NAS5-30430 and NAS5-30440 and DOE ARM Grant DE-A105-90ER61069 is gratefully acknowledged.

APPENDIX A

Spectrum of Cascade Models

The spatial spectrum of the variations in optical depth generated by the cascade model will be derived here. A simple method introduced by Lorenz (1979) for obtaining information about the spectrum of a random process is used. His "poor man's spectral analysis" is based on examining the variance of the running mean of a process at one scale after removing the running mean at twice that scale. The method turns out to be well suited to determining the power spectrum of the multiplicative cascade model.

Consider a stochastic function $f(x)$ whose statistics are homogeneous; that is, they do not depend on position x. The lagged covariance of the function is

$$c(x) = \langle f'(x_0) f'(x_0 + x) \rangle, \tag{A1}$$

where a prime denotes deviation from the mean, and the angular brackets denote averaging over a population of functions all with the same statistics. The covariance $c(x)$ does not depend on position x_0 because the statistics are assumed homogeneous. The power spectrum for the function is obtained from the Fourier transform of the covariance,

$$S(k) = \int_{-\infty}^{\infty} dx e^{-ikx} c(x). \tag{A2}$$

Consider next the averages of $f(x)$ over segments of length L_n, $n = 0, 1, 2, \cdots$,

$$\bar{f}_n = \frac{1}{L_n} \int_0^{L_n} dx f(x), \tag{A3}$$

where the intervals L_n decrease by factors of 2:

$$L_n = 2^{-n} L_0. \tag{A4}$$

The variance of $\bar{f}_n$,

$$V_n = \langle (\bar{f}'_n)^2 \rangle, \tag{A5}$$

can be expressed after a bit of algebra (see, for example, Jenkins and Watts 1967) in terms of the spectrum as

$$V_n = \frac{1}{2\pi} \int_{-\infty}^{\infty} dk \mathcal{F}(kL_n) S(k), \tag{A6}$$

where the "filter" $\mathcal{F}$ is given by

$$\mathcal{F}(z) = \sin^2(z/2)/(z/2)^2. \tag{A7}$$

Lorenz then defines the variance increment

$$\Delta V_n \equiv V_n - V_{n-1}, \tag{A8}$$

which represents the variance of $f(x)$ on scales L_n relative to averages over scale L_{n-1}. The variance increment can also be written as a filtered version of the spectrum,

$$\Delta V_n = \frac{1}{2\pi}\int_{-\infty}^{\infty} dk \mathscr{D}(kL_n)S(k), \tag{A9}$$

with

$$\mathscr{D}(z) = \sin^4(z/2)/(z/2)^2. \tag{A10}$$

The filter function $\mathscr{D}(z)$ peaks near $z \approx \pi$, with width of order 1, and ΔV_n therefore gives the spectral power contained in the octave near wavenumber

$$k_n \equiv \frac{\pi}{L_n}. \tag{A11}$$

The variance increment is particularly informative when the power spectrum behaves like a power law,

$$S(k) \sim k^{-\alpha}, \quad -1 < \alpha < 2. \tag{A12}$$

Equation (A9) then implies that

$$\Delta V_n \sim k_n^{1-\alpha}. \tag{A13}$$

[The extra factor k_n comes from the integral over the width of the filter function. For $\alpha < -1$ or $\alpha > 2$ the behavior of ΔV_n becomes sensitive to the behavior of the spectrum outside the octave around k_n in (A11), and the Lorenz method must be modified to establish power-law behavior.] It follows from (A11) and (A4) that

$$\Delta V_n \sim 2^{n(1-\alpha)} \tag{A14}$$

when the spectrum behaves like a power law. Thus, by identifying power-law behavior of the Lorenz variance increments ΔV_n as in (A14), the exponent α describing the spectrum (A12) can be extracted.

Using the "poor man's spectral analysis," the power spectrum of the multiplicative cascade model defined in section 3 and Fig. 2 can now be determined. After n steps in the cascade process, the optical thickness of one of the segments at the end of the cascade is given by

$$\tau_n = [\prod_{k=1}^{n}(1 \pm f_k)]\tau_v, \tag{A15}$$

where the sign of each factor is chosen randomly. The mean square optical thickness is

$$\langle \tau_n^2 \rangle = [\prod_{k=1}^{n}\langle (1 \pm f_k)^2\rangle]\tau_v^2, \tag{A16}$$

using the fact that each factor varies independently of the other. The variance increment (A8) is

$$\Delta V_n = \langle \tau_n^2 \rangle - \langle \tau_{n-1}^2 \rangle = [\prod_{k=1}^{n-1}\mu_k](\mu_n - 1)\tau_v^2 \tag{A17}$$

with

$$\mu_k \equiv \langle (1 \pm f_k)^2 \rangle = \begin{cases} 1 + f^2, & \text{singular model} \\ 1 + f^2 c^{2k}, & \text{bounded model.} \end{cases} \tag{A18}$$

Substituting (A18) into (A17), the large-n behavior of the two models is identified as

$$\Delta V_n \sim \begin{cases} (1 + f^2)^n, & \text{singular model} \\ c^{2n}, & \text{bounded model.} \end{cases} \tag{A19}$$

Comparing this behavior with (A14), the exponent α in the spectral power law Eq. (A12) is found to be

$$\alpha = \begin{cases} 1 - \log_2(1 + f^2), & \text{singular model} \\ 1 - \log_2 c^2, & \text{bounded model, } c^2 > 1/2. \end{cases} \tag{A20}$$

Note that the singular model exponent α is limited to $0 < \alpha < 1$, since $0 < f < 1$. The bounded cascade model exponent must satisfy $1 < \alpha < 2$ in order for the Lorenz method to be applicable, so that Eq. (A20) is valid only for $1/2 < c^2 < 1$. For $c^2 < 1/2$, a careful analysis of the model behavior reveals that the spectrum is dominated by the spectral power $\sim k^{-2}$ from the step function discontinuities in the optical thickness, and the exponent α therefore plateaus at $\alpha = 2$ for $c^2 < 1/2$. Scaling properties of the bounded cascade model, and generalizations of it, including exponents of the various structure functions, are discussed in some detail in Marshak et al. (1994).

APPENDIX B

Moments of the Optical Depth Distribution

This appendix derives the important result (3.9) for the mean of the logs in the bounded cascade model, and provides an expression for M_2, the variance of the logs. We also give analytic forms for the second and third central moments, m_2 and m_3. We will see that these develop an essential singularity as $c \to 1$. The derivation requires considerable algebraic manipulation and is only sketched here. We give all results in terms of optical depth, but they apply equally to the integrated liquid water.

First consider a specific realization of the model described in Fig. 2 in which the liquid is always moved toward the right. The sequence of pixel op-

tical depths in the first three cascades, then, would look like this:

−,+

−−,−+,+−,++

−−−,−−+,−+−,−++,+−−,+−+,++−,+++,

where the signs indicate whether the optical depth of that pixel is increased or decreased. Wherever a + or − appears, the optical depth at that pixel is multiplied by a factor of $(1 + f_n)$ or $(1 - f_n)$, where n is the cascade step and $f_n = fc^n$. By construction, $\bar{\tau} = \tau_v$ does not change during the cascade. Any other realization differs from this one only by a reshuffling of the pixels at each step, without changing the set of values. To compute the mean of the logarithms, for example, we take the logarithm of each pixel value and average over all pixels. Clearly, such averages do not depend on the order of the pixels. Each pixel value has the form

$$\tau_n = \tau_v \prod_{k=0}^{n} (1 \pm f_k). \tag{B1}$$

Since τ_v multiplies every pixel, it simply shifts the average of the logs by a constant, which we can set to zero by assuming $\tau_v = 1$. Then at the first step the mean logarithm is $[\log(1 - f_0) + \log(1 + f_0)]/2 = \log\sqrt{(1 - f_0^2)}$. At the next step we double the number of terms by including the factors $(1 \pm f_1)$ in the argument of each logarithm, and divide by 4. Performing expansions such as $\log[(1 - f_0)(1 + f_1)] = \log(1 - f_0) + \log(1 + f_1)$ gives a coefficient of 2 in front of each term, reducing the denominator to 2, giving $[\log(1 - f_0^2) + \log(1 - f_1^2)]/2 = \log[\sqrt{(1 - f_0^2)(1 - f_1^2)}]$. Continuing in this way, it is easy to verify (3.9) by induction.

The second logarithmic moment, that is, the variance of $\log(\tau)$ or M_2, can be found similarly by induction. The result is

$$M_2(f) = \sum_{n=0}^{\infty} \left[\log\left(\frac{1 + f_n}{1 - f_n} \right) \Big/ 2 \right]^2. \tag{B2}$$

The solid curve shown in Fig. 3 is the standard deviation of $\log(W)$, which was observed during FIRE to be about 0.39, as shown in Fig. 1. This can be found from (B1) as std dev(log) $= \sqrt{M2}$. Note that a linear rescaling such as (3.1) does not affect this result.

We now consider the moments of τ itself. Since the mean optical depth multiplies every pixel value, the second moment will be proportional to the square of the mean. We can find the proportionality constant by setting $\tau_v = 1$. Then we can write the variance of τ as

$$m_2 \equiv \overline{\tau^2} - 1 = \overline{[\prod_{k=0}^{\infty} (1 \pm f_k)]^2} - 1 = \prod_{k=0}^{\infty} (1 + f_k^2) - 1, \tag{B3}$$

where we have averaged over the random signs. Expanding the products gives terms like

$$f_0^2 + f_1^2 + f_2^2 + f_0^2 f_1^2 + f_0^2 f_2^2 + f_1^2 f_2^2 + f_0^2 f_1^2 f_2^2 + \ldots.$$

Substituting the bounded cascade expression, $f_n = fc^n$, terms like the first three form a geometric series, which sums to

$$\frac{f^2}{1 - c^2}.$$

Similarly, all the bilinear terms form the sum

$$f^4 \sum_{i<j} c^{2i} c^{2j} = \frac{f^4 c^2}{(1 - c^2)(1 - c^4)},$$

where we changed summation variables to $N = j - 1$ and employed the identity

$$\sum_{n=0}^{N} x^n = \frac{1 - x^{N+1}}{1 - x},$$

with $x = c^2$. The following generalization of the geometric series can be proven:

$$\sum_{i_n=n}^{\infty} \cdots \sum_{i_1=1}^{i_2-1} \sum_{i_0=0}^{i_1-1} x^{\sum_{k=0}^{n} i_k} = \prod_{k=0}^{n} b_k(x), \tag{B4}$$

where

$$b_k(x) \equiv \frac{x^k}{1 - x^{k+1}}. \tag{B5}$$

Functions such as (B4) are of importance in number theory where they arise in the theory of partitions of integers, and were first considered by Euler. (See, for example, Hardy and Wright 1979.) Using this result, we find that m_2 can be written in terms of the quantities

$$a_k(f^2, c^2) \equiv f^2 b_k(c^2) = \frac{f^2 c^{2k}}{1 - c^{2k+2}}, \tag{B6}$$

and takes the form

$$m_2 = a_0 + a_0 a_1 + a_0 a_1 a_2 + \cdots, \tag{B7}$$

which can be computed as $a_0(1 + a_1(1 + a_2 \ldots))$ [It is also expressible as a continued fraction.]

Let us now consider the limit of m_2 as $c \to 1$. Using the fact that $(1 - c^{2n+2}) = (1 - c^2)(1 + c^2 + c^4 + \cdots + c^{2n})$, it is apparent that $(1 - c^{2k+2}) \to (1 - c^2)n$, so that $a_n \to a_0/n$. Substituting this into (B7), we obtain

$$m_2 \to a_0 \exp a_0.$$

Since a_0 has a simple pole at $c = 1$, we see that m_2 has an essential singularity at $c = 1$. One implication of this is that the power spectrum of the bounded model ($c < 1$) cannot be analytically continued to the $c = 1$

singular model. This is consistent with the different behavior of the spectral exponents found in appendix A.

The effect of the essential singularity on m_2 is illustrated by comparing Figs. B1a and B1b, which show std dev$(\tau) \equiv \sqrt{m_2}$ for $c = 0.8$ and $c = 0.97$, respectively, computed using (B7) with 5, 10, and 20 terms. When $c = 0.8$, a negligible contribution is made beyond 5 terms, so that the three curves are indistinguishable. Also, the std dev never exceeds three times the mean, even when $f \to 1$. Contrast this with the behavior when $c = 0.97$, when the terms beyond 5 make a large contribution, and the sum converges especially slowly as $f \to 1$. Also, when f exceeds about 0.9, the std dev exceeds 300 times the mean.

After a bit more algebra, one finds that the third central moment can be expressed in terms of the a_n in the form

$$m_3 = 6a_0(a_1 + 4a_1a_2 + 13a_1a_2a_3 + 40a_1a_2a_3a_4 + \cdots). \quad \text{(B8)}$$

The sequence of numerical coefficients in this series satisfies $C_{n+1} = C_n + 3^n$, with $C_1 = 1$, and they grow very rapidly with n. The 20th, for example, is 1 743 392 200. The effect of this rapid growth is illustrated by comparing Figs. B2a and B2b. These show the skewness, namely, $m_3/m_2^{3/2}$, for $c = 0.8$ and $c = 0.97$, respectively, computed using (B7) and (B8) with 5, 10, and 20 terms. When $c = 0.8$, we find a negligible contribution beyond five terms, and the skewness never exceeds 6 even when $f \to 1$. But when $c = 0.97$, the skewness exceeds 6000 before f even reaches 0.8, and the convergence is so slow that even 20 terms may be insufficient. Clearly, as c approaches unity, the skewness diverges even more dramatically than the standard deviation.

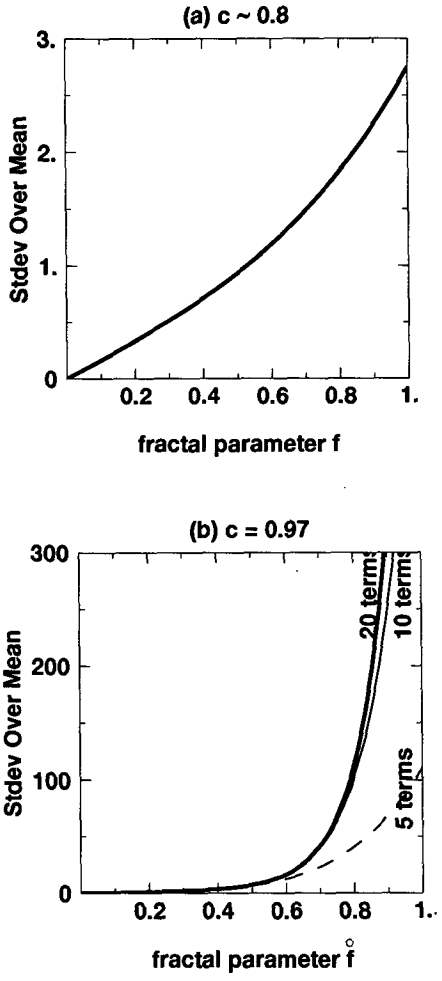

FIG. B1. Standard deviation divided by the mean versus fractal parameter f for the bounded model with (a) $c \approx 0.8$ and $k^{-5/3}$ spectrum and (b) $c = 0.97$ and $k^{-1.09}$ spectrum, according to (A20). The computation was based on Eq. (B7) with 5, 10, and 20 terms included in the sum.

APPENDIX C

Bounds on the Optical Depth

The optical depths in the bounded cascade model are strictly bounded both above and below:

$$\tau_{\min} \leq \tau \leq \tau_{\max}, \quad \text{(C1)}$$

where the extrema are found at two particular pixels, one with

$$\tau_{\max} = \tau_v \prod_{i=0}^{\infty} (1 + f_i) \quad \text{(C2)}$$

and one with $\tau_{\min}$ of the same form with the replacement $(1 + f_i) \to (1 - f_i)$ in every factor of the infinite product. By our linear assumption given in (3.1), the same bounds apply to the vertically integrated liquid water. Since $(1 + f_i) \leq \exp(f_i)$, it is easy to derive a simple upper bound for τ or W:

$$\tau_{\max} \leq \tau_+ \equiv \tau_v \exp\left(\sum_{i=0}^{\infty} f_i\right) = \tau_v \exp[f/(1 - c)] \approx \tau_v \exp(5f), \quad \text{(C3)}$$

where we have used $f_i = fc^i$, summed the geometric series, and set $c \approx 0.8$, as required for a $k^{-5/3}$ spectrum. It is easy to show that

$$\tau_{\max}\tau_{\min} = \tau_{\text{eff}}^2, \quad \text{(C4)}$$

where τ_{eff} is the reduced effective optical thickness defined in (4.2), with the reduction factor χ defined by (3.5). The upper bound on $\tau_{\max}$ implies a lower bound on $\tau_{\min}$, since the product is fixed:

$$\tau_{\min} \geq \tau_- \equiv \tau_{\text{eff}}^2/\tau_+. \quad \text{(C5)}$$

For a typical value of $f = 0.5$, we find $\tau_+ \approx 12\tau_v$

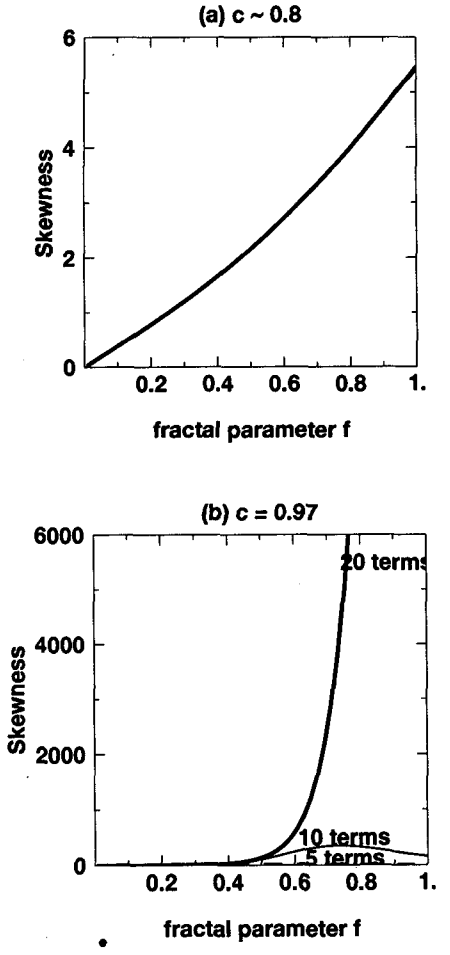

FIG. B2. Skewness versus fractal parameter f for the bounded model with (a) $c \approx 0.8$ and $k^{-5/3}$ spectrum and (b) $c = 0.97$ and $k^{-1.09}$ spectrum. The computation was based on Eq. (B8) with 5, 10, and 20 terms included in the sum.

and $\chi \approx 0.7$, so that $\tau_- \approx 0.5\tau_v/12$. Thus, the ratio τ/τ_v must lie between 1/24 and 12.

APPENDIX D

Analytic Reflection Function for Conservative Scattering

Here we introduce the analytic reflection function for conservative scattering in plane-parallel clouds, given by

$$R(\tau, \theta) = 1 - \frac{\delta(\theta) + (1 - \delta(\theta))e^{-\tau/|\alpha(\theta)|}}{1 + \gamma\tau}, \quad \text{(D1)}$$

where τ is the cloud optical thickness, θ is the solar zenith angle, and α and δ are known functions of θ, related to the backscatter fraction and the escape function, respectively, as given below. This function interpolates between the linear regime at small τ, where $R \approx \beta\tau$, and the known asymptotic behavior at large τ, described, for example, by King and Harshvardhan (1986). Consider first the behavior in the *thick* cloud limit. The exponential term in Eq. (D1) becomes negligible for sufficiently large τ, and the reflection function reduces to the asymptotic form given by King and Harshvardhan [1986, their Eq. (16)] if we set

$$\gamma = (1 - g)/1.428 \approx 0.11, \quad \text{(D2)}$$

where g is the asymmetry parameter, here put equal to 0.843, a value based on the so-called fair weather cumulus (FWC) phase function, appropriate for most water clouds, and if we also set

$$\delta(\theta) = \frac{4}{3}K(\theta)/1.428, \quad \text{(D3)}$$

where K is the escape function for conservative scattering. We find that the escape function for sun angles more than 15° from the horizon ($\theta \leq 75°$) is well approximated by

$$K(\theta) = 0.43 + 0.86\cos\theta, \quad \text{(D4)}$$

where we again assume the FWC phase function. At $\theta = 42°$ we have $\delta = 1$, and (D1) reduces to the two-stream expression (3.8). At larger angles, $\delta < 1$. The $1/\tau$ asymptotic behavior of the transmissivity, $T = 1 - R$, is typical of plane-parallel and other bounded models; T decreases more slowly at large τ for singular fractal models (Lovejoy et al. 1990).

To determine α, we consider the *thin* cloud limit and expand Eq. (D1) about $\tau = 0$. The constant term vanishes, as it should, and if the coefficient of the first-order term is set equal to the backscatter fraction, $\beta(\theta)$, the result can be solved to give

$$\alpha(\theta) = (1 - \delta(\theta)) \Big/ \left(\frac{\beta(\theta)}{\cos(\theta)} - \gamma\right). \quad \text{(D5)}$$

For sun angles more than 15° from the horizon ($\theta \leq 75°$) we find that the backscatter fraction is well approximated by

$$\beta(\theta) = 0.37 - 0.32\sqrt{[\cos(\theta)(2 - \cos(\theta))]}, \quad \text{(D6)}$$

for the FWC phase function.

At $\theta = 60°$, which is typical of marine stratocumulus observed during FIRE, the preceding equations give $\delta \approx 0.8$, $\beta \approx 0.093$, and $\alpha \approx 2.6$.

REFERENCES

Albrecht, B. A., D. A. Randall, and S. Nicholls, 1988: Observations of marine stratocumulus clouds during FIRE. *Bull. Amer. Meteor. Soc.*, **69**, 618–626.

Barker, H. W., and J. A. Davies, 1992: Radiative transfer, cloud structure, and the characteristics of satellite radiance wavenumber spectra. *Remote Sens. Environ.*, **42**, 51–64.

Cahalan, R. F., 1989: Overview of fractal clouds. *Advances in Remote Sensing Retrieval Methods*, A. Deepak, 371–388.

——, 1992: Kuwait oil fires as seen by Landsat. *J. Geophys. Res.*, **97**, 14 565–14 571.

——, and J. H. Joseph, 1989: Fractal statistics of cloud fields. *Mon. Wea. Rev.*, **117,** 261–272.
——, and J. B. Snider, 1989: Marine stratocumulus structure. *Remote Sens. Environ.*, **28,** 95–107.
——, and W. J. Wiscombe, 1993: Impact of cloud structure on climate. *Current Problems in Atmospheric Radiation,* S. Keevallik and O. Karner, Eds., A. Deepak, 120–123.
——, W. Ridgway, W. J. Wiscombe, S. Gollmer, and Harshvardhan, 1994: Independent pixel and Monte Carlo estimates of stratocumulus albedo. *J. Atmos. Sci.,* in press.
Coakley, J., 1991: Reflectivities of uniform and broken layered clouds. *Tellus,* **43B,** 420–433.
Davis, A., P. Gabriel, S. Lovejoy, D. Schertzer, and G. Austin, 1990: Discrete angle radiative transfer III: Numerical results and meteorological applications. *J. Geophys. Res.*, **95,** 11 729–11 742.
——, S. Lovejoy, and D. Schertzer, 1991: Discrete angle radiative transfer in a multifractal medium. *SPIE Proc.,* **58,** 3759.
Durkee, P., 1988: The influence of continental sources of aerosols on the marine stratocumulus during FIRE IFO-1. *Proc. FIRE Science Results 1988,* Vail, CO, NASA Conf. Publ. 3083, 151–155.
Fairall, C. W., R. E. Rabadi, and J. Snider, 1990: Estimating integrated cloud liquid water from extended time observations of solar irradiance. *Proc. FIRE Science Results 1988,* Vail, CO, NASA Conf. Publ. 3083, 307–312.
Gage, S. K., and D. G. Nastrom, 1986: Theoretical interpretation of atmospheric wavenumber spectra of wind and temperature observed by commercial aircraft during GASP. *J. Atmos. Sci.,* **43,** 729–740.
Hardy, G. H., and E. M. Wright, 1979: *An Introduction to the Theory of Numbers.* Oxford Science Publications, 5th ed., Oxford University Press, 426 pp.
Harrison, E. F., P. Minnis, B. R. Barkstrom, V. Ramanathan, R. D. Cess, and G. G. Gibson, 1990: Seasonal variation of cloud radiative forcing derived from the Earth Radiation Budget Experiment. *J. Geophys. Res.*, **95,** 18 687–18 703.
Harshvardhan, and J. Weinman, 1982: Infrared radiative transfer through a regular array of cuboidal clouds. *J. Atmos. Sci.*, **39,** 431–439.
——, and D. A. Randall, 1985: Comments on "The parameterization of radiation for numerical weather prediction and climate models." *Mon. Wea. Rev.*, **113,** 1832–1833.
Hartmann, D. L., and D. A. Short, 1980: On the use of earth radiation budget statistics for studies of clouds and climate. *J. Atmos. Sci.,* **37,** 1233–1250.
——, M. E. Ockert-Bell, and M. L. Michelsen, 1992: The effect of cloud type on earth's energy balance: Global analysis. *J. Climate,* **5,** 1281–1304.
Hogg, D. C., F. O. Guiraud, J. B. Snider, M. T. Decker, and E. R. Westwater, 1983: A steerable dual-channel microwave radiometer for measurement of water vapor and liquid in the troposphere. *J. Climate Appl. Meteor.*, **22,** 789–806.
Jenkins, G. M., and D. G. Watts, 1967: *Spectral Analysis and Its Applications,* chap. 6. Holden-Day, 525 pp.
Jensen, J. L. W. V., 1906: Sur les fonctions convexes et les inégalitiés entre les valeurs moyennes. *Acta Math.*, **30,** 175–193.
King, M. D., and Harshvardhan, 1986: Comparative accuracy of selected multiple scattering approximations. *J. Atmos. Sci.,* **43,** 784–801.
Kraichnan, R. H., 1967: Inertial ranges in two-dimensional turbulence. *Phys. Fluids,* **10,** 1417–1423.
Lilly, D. K., 1989: Two-dimensional turbulence generated by energy sources at two scales. *J. Atmos. Sci.,* **46,** 2026–2030.
Lorenz, E. N., 1979: Forced and free variations of weather and climate. *J. Atmos. Sci.,* **36,** 1367–1376.
Lovejoy, S., 1982: Area–perimeter relation for rain and cloud areas. *Science,* **216,** 185–187.
——, A. Davis, P. Gabriel, D. Schertzer, and G. L. Austin, 1990: Discrete angle radiative transfer I: Scaling and similarity, universality and diffusion. *J. Geophys. Res.*, **95,** 11 699–11 715.
Mandelbrot, B., 1983: *The Fractal Geometry of Nature.* W. H. Freeman, 460 pp.
——, 1986: Self-affine fractal sets, Parts I, II, and III. *Fractals in Physics,* L. Pietronello and E. Tosatti, Eds., Elsevier, 3–28.
Marshak, A., A. Davis, R. F. Cahalan, and W. J. Wiscombe, 1994: Bounded cascade models as non-stationary multifractals. *Phys. Rev.*, **E49,** 55–79.
McKee, T. B., and S. K. Cox, 1974: Scattering of visible radiation by finite clouds. *J. Atmos. Sci.*, **31,** 1885–1892.
McVean, M. K., and S. Nicholls, 1988: A fine-resolution, two-dimensional numerical study of a cloud-capped boundary layer. *Proc. Tenth Int. Cloud Physics Conf.,* Bad-Hamburg, Germany, IAMAP, 425–427.
Mineart, G. M., 1988: Multispectral satellite analysis of marine stratocumulus cloud microphysics. M.S. thesis, Naval Postgraduate School, Monterey, CA, 138 pp.
Minnis, P., P. W. Heck, D. F. Young, C. W. Fairall, and J. B. Snider, 1992: Stratocumulus cloud properties derived from simultaneous satellite and island-based instrumentation during FIRE. *J. Appl. Meteor.*, **31,** 317–339.
Nakajima, T., M. D. King, J. D. Spinhirne, and L. F. Radke, 1991: Determination of the optical thickness and effective particle radius of clouds from reflected solar radiation measurements. Part II: Marine stratocumulus observations. *J. Atmos. Sci.*, **48,** 728–750.
Ramanathan, V., R. D. Cess, E. F. Harrison, P. Minnis, B. R. Barkstrom, E. Ahmad, and D. Hartmann, 1989: Cloud–radiative forcing and climate: Results from the Earth Radiation Budget Experiment. *Science,* **243,** 57–63.
Rhys, F. S., and A. Waldvogel, 1986: Fractal shape of hail clouds. *Phys. Rev. Lett.*, **56,** 784–787.
Rossow, W. B., and R. A. Schiffer, 1991: ISCCP cloud data products. *Bull. Amer. Meteor. Soc.*, **72,** 2–20.
Schertzer, D., and S. Lovejoy, 1987: Physically-based rain and cloud modeling by anisotropic, multiplicative turbulent cascades. *J. Geophys. Res.*, **92,** 9693–9714.
Short, D. A., G. R. North, T. D. Bess, and G. L. Smith, 1984: Infrared parameterization and simple climate models. *J. Climate Appl. Meteor.*, **23,** 1222–1233.
Snider, J. B., 1988: Estimated accuracy of ground-based liquid water measurements during FIRE. *Proc. FIRE Science Results 1988,* Vail, CO, NASA Conf. Publ. 3083, 289–292.
Stephens, G. L., 1976: The transfer of radiation through vertically non-uniform stratocumulus clouds. *Contrib. Phys. Atmos.*, **49,** 237–253.
——, 1985: Reply. *Mon. Wea. Rev.*, **113,** 1834–1835.
——, 1988a: Radiative transfer through randomly fluctuating optical media, Part I. *J. Atmos. Sci.*, **45,** 1818–1836.
——, 1988b: Radiative transfer through randomly fluctuating optical media, Part II. *J. Atmos. Sci.*, **45,** 1837–1848.
——, P. M. Gabriel, and S.-C. Tsay, 1991: Statistical radiative transport in one-dimensional media and its application to the terrestrial atmosphere. *Trans. Theory Stat. Phys.*, **20,** 139–175.
Welander, P., 1955: Studies on the general development of motion in a two-dimensional ideal fluid. *Tellus,* **7,** 141–156.
Welch, R., and B. A. Wielicki, 1985: A radiative parameterization of stratocumulus cloud fields. *J. Atmos. Sci.*, **42,** 2888–2897.
Wetherald, R. T., and S. Manabe, 1980: Cloud cover and climate sensitivity. *J. Atmos. Sci.*, **37,** 1485–1510.
Wielicki, B. A., and L. Parker, 1992: The determination of cloud cover from satellite sensors: The effect of sensor spatial resolution. *J. Geophys. Res.*, **97,** 12 799–12 823.